

Motion based cable integrity limits for quadrant  
assisted pull-in operations on submarine inter-array  
cables

---

Daan Sotiriadis

*April 5, 2020*  
Version: Final



Delft University of Technology



Faculty of Mechanical, Maritime & Materials  
Engineering  
Department of hydrodynamics



Boskalis Westminster BV.  
Subsea Cables  
Hydrodynamics

MSc. graduation thesis

**Motion based cable integrity limits for quadrant  
assisted pull-in operations on submarine  
inter-array cables**

Daan Sotiriadis

**Thesis Committee**

*TU Delft Supervisors*

**Dr. Ir. P.R. Wellens**

Ship Hydromechanics & Structures  
Mechanical, Maritime & Materials Engineering

**Ir. P. Xu**

Ship Hydromechanics & Structures  
Mechanical, Maritime & Materials Engineering

**Dr. Ir. X. Jiang**

Transport Engineering & Logistics  
Mechanical, Maritime & Materials Engineering

*Boskalis Supervisors*

**Ir. M.A. Beerens**

Marine Engineering  
Boskalis Subsea Cables

**MSc. R. Beindorff**

Marine Engineering  
Boskalis Subsea Cables

April 5, 2020



# Abstract

The installation of subsea cables connecting offshore wind turbines to the grid is a delicate process. This is especially the case for the operation of connecting the second end of the cable to the turbine. The applied method of using a quadrant means that in the workability analyses, multibody dynamics, line dynamics and sea state dynamics need to be combined, resulting in lengthy simulation requirements. The objective of this thesis is to determine vessel motion based limits to cable integrity in order to simplify workability analyses. This method allows the problem to be analyzed in the frequency domain, resulting in computational efficiency gains.

In order to arrive at the desired result a literature study is performed regarding cable loading and cable failure modes encountered during quadrant assisted cable pull-ins. On that basis a detailed investigation into the relations between vessel motion and mechanical cable responses is carried out. To achieve this, a representative cable and a set of high but realistically encountered sea states are simulated. The obtained relations are then compared to the cable integrity limits for curvature, tension and compression to acquire limits expressed in terms of motion parameters such as acceleration, velocity and displacement.

The results from these simulations show that: 1) maximum cable tension is closely correlated to upward heave velocity of the crane tip, 2) maximum cable compression is closely correlated to downward heave velocity, 3) maximum curvature is most closely correlated to downward heave velocity. It is concluded from the results that the cable response can be determined from the crane tip heave motion, which in turn is known from the vessel motions. This means that analysis of such a problem is possible in the frequency domain.

As the results show that heave motion is governing in cable failure, heave compensation in the crane is recommended for the operations considered. In addition, an enhancement of the analysis process is proposed by extracting the linear relations and vessel motion limits from a small set of time domain simulations and assessing the situation thoroughly in a frequency domain analysis.

The configurations considered exclude any effects added by cable protection systems or interaction effects with rigid bodies in the vicinity of the cable. Even though the analysis process is generally applicable and constitutes a significant improvement in computational load, the obtained relations may be generalized further by implementing a closed formula relating vessel motion to cable failure, or application of the cable protection system to the assessed configuration. Additional research in these directions is encouraged.



# Preface

This thesis on 'Motion based cable integrity limits for quadrant assisted pull-in operations on submarine inter-array cables' concludes my Offshore & Dredging Engineering master degree education at Delft University of Technology. It was made possible by the graduation internship provided to me by Boskalis Subsea Cables. The supportive environment I found there was invaluable in helping me succeed in this assignment.

I would like to express my gratitude to my supervisors Peter Wellens, Maarten Beerens and Ruud Beindorff. The optimism, feedback and insight they provided throughout the process of writing this thesis has to a large extent helped me perform the research and write the document.

Many thanks also go out to Peter Jacobs for the many drives to the office, the group of graduate interns at Boskalis for providing feedback, support and a pleasant atmosphere during lunch, and my girlfriend, friends and family for supporting me throughout the process.

Finally, I would like to thank the reader for taking interest in the subject described in this thesis. May you have a pleasant read and find the information you are looking for.

Daan Sotiriadis  
Delft, April 2020



# Contents

<b>1</b>	<b>Introduction</b>	<b>1</b>
1.1	Cable laying . . . . .	1
1.2	Operability & Workability . . . . .	2
<b>2</b>	<b>Problem definition</b>	<b>3</b>
2.1	Objectives . . . . .	3
2.2	Research questions . . . . .	4
2.3	Scope . . . . .	4
2.4	Literature . . . . .	5
2.5	Reading guide . . . . .	5
<b>3</b>	<b>Quadrant assisted cable pull-in</b>	<b>7</b>
3.1	Process . . . . .	7
3.2	Cable . . . . .	8
3.3	Vessel . . . . .	11
3.4	Equipment . . . . .	11
3.5	Environment . . . . .	12
<b>4</b>	<b>Literature</b>	<b>15</b>
4.1	Offshore lifting by floating cranes . . . . .	15
4.2	Catenary mooring systems . . . . .	18
4.3	Cable failure modes . . . . .	20
<b>5</b>	<b>Current analysis methodology</b>	<b>25</b>
5.1	Simulation steps . . . . .	25
5.2	Modeling of cables . . . . .	26
5.3	Environmental loading . . . . .	27
5.4	Calculation method . . . . .	28
5.5	Workability assessment . . . . .	28
5.6	Method improvement . . . . .	29
<b>6</b>	<b>Methodology</b>	<b>31</b>
6.1	Modeling and analysis process . . . . .	31
6.2	Configuration . . . . .	32
6.3	Sea states . . . . .	33
6.4	Vessel response . . . . .	34
6.5	Static and dynamic analysis . . . . .	35
6.6	Results . . . . .	36

6.7	Limits . . . . .	37
6.8	Parameter variation . . . . .	38
<b>7</b>	<b>OrcaFlex modeling</b>	<b>39</b>
7.1	Model elements . . . . .	39
7.2	Interactions . . . . .	41
7.3	Verification . . . . .	42
<b>8</b>	<b>Results</b>	<b>45</b>
8.1	Normal cable laying . . . . .	45
8.2	Preliminary observations . . . . .	46
8.3	Relations . . . . .	47
8.4	Limits . . . . .	49
8.5	Wave loading . . . . .	50
8.6	Parameter variations . . . . .	52
<b>9</b>	<b>Conclusions &amp; recommendations</b>	<b>55</b>
9.1	Discussion . . . . .	55
9.2	Conclusions . . . . .	56
9.3	Implications . . . . .	59
	<b>Bibliography</b>	<b>63</b>
	<b>Appendices</b>	<b>65</b>
<b>A</b>	<b>Vessel motion analysis Stemat Spirit</b>	<b>67</b>
<b>B</b>	<b>Hydrodynamic interaction</b>	<b>71</b>
<b>C</b>	<b>Statistic analysis</b>	<b>73</b>
<b>D</b>	<b>Sensitivity study</b>	<b>77</b>
<b>E</b>	<b>Glossary of terms</b>	<b>83</b>
<b>F</b>	<b>Figures and Tables</b>	<b>87</b>

# Introduction

” *Don't touch me I'm a real live wire.*

— **Talking heads**  
(Rock band)

The sustained increase of the global population and the prosperity growth in developing regions feeds an ever increasing demand for energy worldwide. With traditional sources such as fossil fuels running into limitations regarding supply and environmental impact in the near future, a shift towards renewable sources is gaining momentum. In addition to solar power and bio fuels, wind generated power is one of the main sources of renewable energy, especially in Europe (Komusanac et al., 2019).

With limited space on land and a stronger and more steady energy source at sea, locating wind farms offshore is becoming the trend. To be able to connect the wind turbines in these wind farms to each other, their substations and the consumers, a large number of cables runs along the seabed. While the developments towards offshore wind are promising, total costs of energy of offshore wind sources need to come down to be able to compete with fossil fuels. Optimizing the installation of the subsea cables can contribute to this.

The installation of subsea cables between offshore wind turbines is not an easy task as these inter-array cables are delicate products and need to be handled with care. Meanwhile, subsea cable damages still account for disproportionate amounts of financial damage in wind farm operation and it is imperative that this is reduced. Proper cable installation is an absolute necessity to achieve this. The difficulty is that the process takes place at sea, where the cable and installation vessel are at the mercy of the waves, winds and currents.

## 1.1 Cable laying

Normal cable laying is a continuous process in which the cable hangs of the back of an installation vessel with one end of the cable installed and anchored to the seabed. The cable lay vessel (CLV) then proceeds to follow the intended route of the cable while keeping a certain tension on it. The other end of the cable is released out from the back of the vessel, guided by a chute or stinger to maintain a minimum bending radius (MBR). Under influence of gravity the cable will take on a catenary shape down to the seabed where it will settle in the intended position, after which it can be trenched, covered or left as it is.

While the bulk of the cable laying is carried out in a continuous fashion, some operations in cable installation differ from this process and require special attention. First and second end pull-ins are performed to connect the respective cable ends to the turbines, offshore jointing can be carried out to connect two cables to each other and tool overboarding can be used when a cable needs to be trenched or covered. These activities are called complex operations and one of them, the second end or quadrant assisted pull-in, will be the focus of this thesis.

## 1.2 Operability & Workability

The complex operations as well as the continuous cable lay process are subject to limits with respect to the conditions at which they can be performed. The set of constraining conditions determine the operability of the activity. The cable integrity needs to be guaranteed at all times as installing a damaged cable would require extra activities to recover, repair and re-install the cable, leading to delays and extra costs. Workability analyses are performed to assess the maximum wind, wave and current conditions at which the cable integrity remains guaranteed. By comparing the limits to actual weather forecasts a decision is made whether or not the operation can be performed. The amount of time an operation can be carried out in a certain period of the year is what defines the workability.

# Problem definition

“ *Computers are useless, they can only give you answers*

— Pablo Picasso

The workability assessment of the quadrant assisted pull-in operation is a problem with many components, variables and degrees of freedom. The problem is highly nonlinear which means that the analysis involves a lot of effort. The current methodology is to run a set of time domain simulations in a commercial software package called OrcaFlex™. The limit states are expressed in terms of discretized values of the significant wave height ( $H_s$ ), spectral peak period ( $T_p$ ) and directional angle, in line with industry guidelines. Running these simulations is computationally very intensive, time consuming and expensive. In addition, this approach reduces the amount of required knowledge about the physical processes at work which means that no new insights are generated that might improve the situation. Moreover, in the current methodology some inaccuracies are incorporated that potentially negatively impact the workability of the system. These inaccuracies originate from the discretization of the limit sea states as well as conservatism in analysis and application of the limit states. Expressing limit states in terms of vessel motions would address these issues and is encouraged by the industry (DNV-GL, 2016).

## 2.1 Objectives

Taking the aforementioned into account, the main objective of this thesis is to:

**Define 'vessel motion' based operation limits for quadrant assisted pull-in operations for which cable integrity is preserved.**

Finding these limits would make it possible to analyze the problem in a frequency domain assessment. In doing so it is aimed to achieve:

1. Generation of knowledge and insight in the physics involved in quadrant assisted cable pull-in operations leading to an improvement in engineering methodology.
2. A linearization of the problem leading to a reduction in engineering intensity.

3. A reduced need for time domain analyses leading to lower computational requirements for the analysis of the problem.
4. Identifying key areas for improvement of workability in the second end pull-in process.

## 2.2 Research questions

From the objectives the main research question and subquestions are formulated:

### **What are the relations between vessel motions and cable integrity limits for the quadrant assisted pull-in operation?**

1. What physical properties and processes play a significant role in cable loading during quadrant assisted pull-in?
2. Which cable failure modes may be activated by the operation and what limits on cable response do they impose?
3. What are the relations between vessel motion and cable response?
4. What are the governing limiting motion conditions of the vessel on cable integrity?

## 2.3 Scope

This thesis is intended to achieve the objectives and answer the questions posed above primarily for the second end pull-in of inter-array cables. For the continuous cable lay process such a relation is already formulated (Loos, 2017). Among the complex operations, the second end pull-in is the most extensive operation that is executed frequently and thus the most beneficial to analyse. Included in the scope of this thesis are the vessel motions in both regular and irregular wave conditions, as well as direct wave loading on submerged parts of cable and quadrant.

Failure modes of the operation other than those related to cable integrity are not considered in this thesis. The efforts are focused on the cable as it is a vulnerable product. The cable limits will mostly be reached before other failure modes are activated. In addition to this, the consequences of cable failure are more severe than those of many other failure modes in terms of cost exceedances and time delays.

Excluded from this research are the complex operations of offshore jointing of cables and the overboarding of tools involving cables. These are so infrequently executed and of such magnitude that it warrants a full analysis every time and it will never be executed in sea states close to the workability limit.

Finally, wind and current loading are not regarded in this thesis as they represent low dynamic loading in the limiting sea states.

## 2.4 Literature

The workability analysis of cable laying operations is experiencing a slow transition away from brute force analysis methods. A driving force of change in the business are the joint industry projects (JIPs) (DNV-GL, 2016; DNV-GL, 2014). These state that motion based criteria may be applied as an alternative to the currently applied  $H_s$ ,  $T_p$  and direction limits based on full time domain irregular wave excitation simulations. This has sparked research to obtain these motion based criteria. This thesis may be viewed as a continuation of the work of Loos (2017), who formulated a relation between vessel motion and cable integrity limits for the continuous cable laying process. It is concluded that the limiting failure mode for the cable lay process is compression near the touchdown point, where the chute velocity in the axial cable direction is found to be governing. This axial motion direction will also be investigated in this thesis.

With respect to cable properties, insight is provided in the high voltage alternating current (HVAC) cable compression limit by Reda et al. (2016). This has urged the industry to move from a conservative zero compression condition to more realistic ranges. In bending behavior a transition is made from the application of linear bending stiffness towards using nonlinear relations (Maioli, 2016) and hysteresis behavior (Tan et al., 2009), incorporating dependence on curvature magnitude and load frequency. This is essential to accurately determine cable limits and responses. Literature on motion behavior of offshore lifting operations is available in several iterations. Hannan and Bai (2016) describe the nonlinear dynamics of a fully submerged heavy payload, suspended by a crane barge. By means of numerical simulations, several nonlinear effects are observed to significantly influence payload motion. Eng et al. (2008) devised a method for estimating the hydrodynamic coefficients for an underwater vehicle using a free decay pendulum test. The results showed good agreement with simulation results. Sarkar and Gudmestad (2010) provides a discussion on splash zone passage of subsea structures for installation. It incorporates the free surface proximity effect on added mass of flat surfaces, winch speeds and crane stiffness, but emphasizes the selection of hydrodynamic coefficients.

## 2.5 Reading guide

The way to go about attaining the objectives and answering the research questions is visualized in the flowchart in Figure 2.1.

In the preliminary phase the problem is defined, the objectives are determined and the research questions are formulated. In order to be able to do this the analysis is started in Chapter 3 by determining the relevant steps in the second end pull in operation including a description of the key elements playing a role in it.

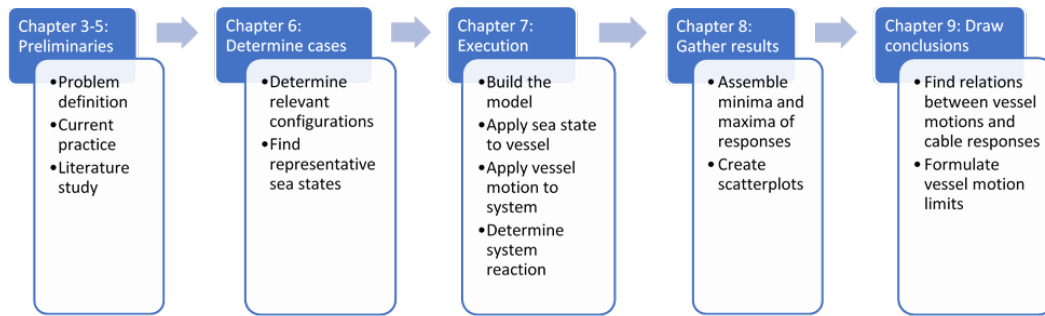


**Figure 2.1.:** Flowchart of the analysis process.

In Chapter 4 a literature study is performed after which the current analysis method is described in Chapter 5. From this the existing inefficiencies and knowledge deficiencies were determined, leading to the formulation of the objectives and research questions in chapter 2.

The analysis process for the identified problems and objectives is presented in Chapter 6. The configurations in the critical stages are identified, relevant sea states are determined, static and dynamic analysis methods are described and the processing and selection of the relevant results is presented.

In Chapter 7 the system configuration is modeled in such a way that the analysis cases can be executed. The cable-quadrant system is implemented in a software package named Orcaflex. In Orcaflex the sea states are imposed on the vessel, which in turn will excite the cable-quadrant model and generate a response in terms of a mechanical cable parameters of interest: curvature, tension and compression. In parallel, a python model is built that is used to verify the methods implemented in Orcaflex and to gain insight into the mechanics and effects at work.

The data generated in the execution phase is collected, processed and visualized in Chapter 8 after which relations and vessel motion limits are determined and discussed in chapter 9.

## Quadrant assisted cable pull-in

A variety of factors define the activity and the workability of the second end cable pull-in. The process itself determines which steps are critical; the cable determines the hard limits and the vessel; equipment and loading conditions determine what the ultimate workability will be. Each of these boundary conditions is considered in this chapter.

### 3.1 Process

The process that is executed to perform the second end cable pull-in consist of several steps, or snapshots, as indicated below in Figure 3.1-3.5. While in reality the installation sequence is a continuous process, these snapshots represent system configurations at fixed amounts of progress in the installation process. In this way, it is possible to assess the system at discrete situations that are deemed critical. **The snapshot approach is an important concept and is used extensively throughout the industry and this document.**

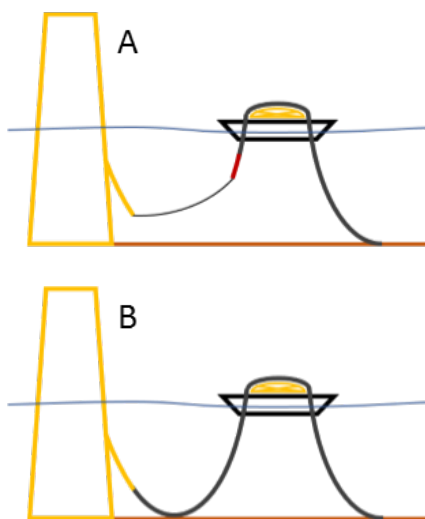


**Figure 3.1.:** Snapshot A

The free end of the cable is fitted with a cable protection system (CPS) to protect the cable against rubble, sharp edges, MBR exceedance and fatigue between the entry point and the buried bulk of the cable. The free end is pulled in toward the entry point in the turbine foundation by a winch wire.

**Figure 3.2.:** Snapshot B

The CPS is locked in the entry point. The tension on the winch wire activates a quick release mechanism that enables the cable to be pulled through the CPS.

In stages A and B the situation closely resembles normal cable laying as the cable hangs off the stern of the vessel over a deployment chute. The cable will take on a catenary shape under influence of gravity. Even though the vessel has no forward speed in this case and there are two stretches of cable hanging off the chute, the cable integrity can be assessed by means of axial cable loading as is applicable to normal cable laying (Loos, 2017). In stages C and D this assessment is not valid

anymore as the quadrant is included. This extra body increases the degrees of freedom of the system, altering the behavior drastically. The suspended quadrant will exhibit different motion behavior than the chute, leading to a different cable response. Once the quadrant enters the water it becomes subject to hydrodynamic loading, altering the cable response even further. Stage E is an all together different situation as the catenaries have all but disappeared. There is no way for the cable to absorb large motions of the quadrant. The quadrant motion generated by the imposed suspension point motion will therefore lead to significantly altered cable responses. The proximity of the seabed also means that impacting of the quadrant and cable on the seabed is a factor contributing to the cable integrity limits. A more detailed description of snapshots C, D and E will be given in Section 6.2.

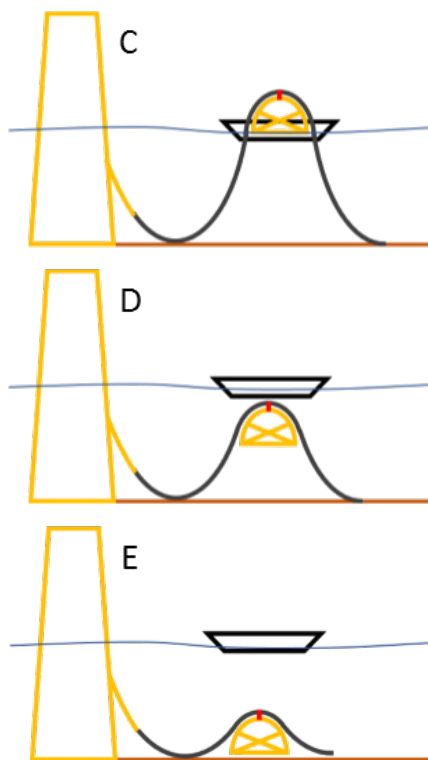


**Figure 3.3.:** Snapshot C

The excess cable length on board the ship is suspended on a quadrant: a semi-circular guide frame, that is gently lowered by a crane. By simultaneously pulling in the cable into the foundation the slack is tightened.

**Figure 3.4.:** Snapshot D

The crane lowers the quadrant through the splash zone, while the cable is pulled in.

**Figure 3.5.:** Snapshot E

At the bottom, the quadrant is tilted sideways, releasing the suspended cable on to the seabed. The remaining slack is pulled in, after which the cable end is clamped. The installed cable can now be buried up to the CPS.

## 3.2 Cable

All subsea cables have a similar basic structure. Whether the cable is used for communication or for power transfer, the main task is fulfilled by the conductive inner core. Around the core several layers of electrically non-conductive layers are applied to insulate the cable from potential impact from the outside environment. In order to ensure the non-conductive properties of the insulation layer a watertight metallic layer is applied. These sheaths are often made from lead or lead alloys, as this provides an excellent barrier against moisture intrusion. In order to protect the inner structure of the cable against mechanical loads, armoring wires are present in the cable. These armor wires take the majority of tension and bending loads during

laying operations and provide protection to all sorts of mechanical loads once the cable is in place (Worzyk, 2009).

A large variety of cable types is available, with an equally large variety in applications. A very notable distinction can be made between alternating current (AC) cables and direct current (DC) cables, as is indicated in figures 3.6 and 3.7. Cables carrying DC consist of a single conductive core wrapped in the aforementioned isolation and armor layers. These cables are the best choice for long distance energy transport as the energy loss over the length is low. AC cables consist of three conductive cores. Each core is individually insulated and protected against water intrusion but share a common wire armor for mechanical load absorption. AC cables are the best choice for shorter lengths as energy is normally generated in AC form. Omitting the costly transformers for conversion to DC in these cases outweighs the limited energy losses. Alternatively, the AC circuit can be completed by installing three separate cables. Most high voltage cables are electrically insulated by cross linked



**Figure 3.6.:** DC cable structure (courtesy of Nexans).



**Figure 3.7.:** AC cable structure (courtesy of Nexans).

polyethylene (XLPE). Polyethylene (PE) is a hydrocarbon consisting of long chains. It has excellent insulating properties but melts at around 80 °C. Cross linking the molecular chains of the material creates XLPE, which pyrolyses at 300 °C instead of melting. This has made XLPE the industry standard insulation system.

Armoring of the cable generally consists of steel wiring lining the outer perimeter of the cable. The steel wires are wound around the core creating a helical wire cage. The armoring functions as the primary load bearing element. Multiple armoring solutions exist, including but not limited to: single helical, double helical, counter-helical and combinations of long and short pitch wiring. Each armor type influences the overall properties significantly which makes it suited to specific conditions.

While subsea cables are used in many applications, the second end pull-in operation is mostly performed on inter-array cables in offshore wind farms. These cables are

needed to connect the offshore wind turbines to each other, the electrical substation and the onshore grid. The generators on the wind turbine generate alternating current, which need to be transported to the substation. Only at the substation can the current be converted to direct current if that is required. The inter-array cables therefore are three core HVAC type cables with XLPE insulation and single helical, long pitch, steel wire armor, as depicted in Figure 3.7. The relevant properties of a representative cable are listed in Table 3.1. A more description of the cable failure modes is discussed in Section 4.3.

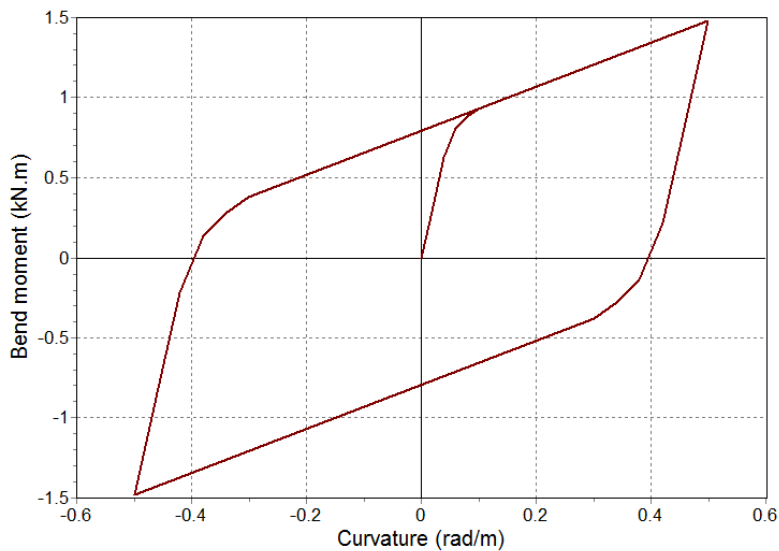


**Figure 3.8.:** Nonlinear bending stiffness implemented in this thesis.

An important parameter in the analysis of cable dynamics is the cable bending stiffness. It is a property that is dependent on the loading conditions. As a result of the different components that make up the cable, stick-slip behavior occurs. This causes the bending stiffness to vary non-linearly with respect to the cable curvature. The bending stiffness for the representative cable is described by the hysteresis loop provided in Figure 3.8. This means that the bending stiffness not only differs nonlinearly with the curvature, but is also dependent on whether the cable is being loaded or unloaded.

**Table 3.1.:** Representative properties of inter-array cables. The values presented here will be used throughout this thesis.

Voltage	33	[kV]
Outer diameter	124	[mm]
Weight in air	25.22	[kg/m]
Weight in sea water	14.65	[kg/m]
Axial stiffness	284	[MN]
Torsional stiffness clockwise	1.27	[kNm <sup>2</sup> /deg]
Torsional stiffness counter clockwise	0.42	[kNm <sup>2</sup> /deg]
MBR under tension	2600	[mm]
Max. axial tension	110	[kN]
Max. compression	10	[kN]
Max. sidewall pressure	50	[kN/m]
Max. squeeze load	136	[kN/m]

### 3.3 Vessel

The vessels used in cable installation need to be able to carry out all the activities required to fully install a cable: the first end pull-in, the bulk cable laying and the second end pull-in. For adequate handling capability they are fitted with a set of specialized equipment. It consists of at least a cable carousel for storage, a payout chute to maintain MBR, a quadrant to suspend the cable during the second end pull-in including a rail for the on deck handling and a crane or A-frame to carry out the lifting activities.

The vessel under consideration is the Stemat Spirit, a CLV with a cable carrying capacity of 4600 tons. The cable is stored on a rotating cable carousel located in the middle of the deck. The vessel features a crane capable of lifting 140 tons, which is more than enough for handling the cable and quadrant weight during second end pull-in. The quadrant rail is located at the starboard aft of the vessel and ends in the payout chute. During continuous cable laying the cable is fed along the rail to the chute and paid out by the carousel. During the second end pull-in the quadrant moves along this rail until it is lifted by the crane. A more detailed description of the vessel is given in Appendix A.

### 3.4 Equipment

In order to tie in the cable to the wind turbine foundation from the deck of a CLV, a stretch of excess length is required. This stretch of cable hangs off the chute on the back of the ship for the already installed end. The free end is laid out on deck horizontally and run around a semicircular guide frame. This guide frame is called a quadrant and serves as the suspension frame for the cable during the entire operation. The quadrant is in turn suspended on lifting arrangement and lowered to the seabed while the end of the cable is pulled in.

During this process the cable needs to be supported by the quadrant and remain

securely in place. The heavy duty steel frame is fitted with upright edges along the circumference that prevent sideways motion off the frame. In the direction of the curvature the cable needs to be able to slide over the curved frame. To facilitate this the quadrant is fitted with rollers. Once the quadrant reaches the bottom it needs to be tilted to release the cable onto the seabed. During the entire process the cable integrity may not be compromised by the quadrant. The structure is designed such that MBR, maximum sidewall pressure and maximum crushing load are not exceeded at any time. The radius of the quadrant and the spacing of the rollers ensure these conditions are met. The quadrant is displayed in Figure 3.9 and the relevant properties are given in Table 3.2.



**Figure 3.9.:** Quadrant

**Table 3.2.:** Properties of 3.2 m MBR quadrant (BSCF, 2018)

Self weight	3.5	[T]
Cable pay load	5.5	[T]
MBR	3.2	[m]
Max. cable diameter	350	[mm]
Number of guide rollers	12	[-]

## 3.5 Environment

When venturing out to sea there are three main environmental effects that need to be taken into account: wind, current and waves. Each of these effects generate loads and motions on any structure or vessel it acts upon.

Ocean currents can consist of multiple phenomena. Tidal motions, the ocean circulation system, water density differences and wind loading all contribute to current generation (Journée et al., 2015). Velocity and direction of the current generally vary slowly, making it reasonable to consider current as a steady effect. In cases where station keeping is important the loads generated by this steady forcing need to be dissipated through a mooring system or a dynamic positioning system. Deep currents can also induce static loads in catenaries and riser systems. For higher flow velocities dynamic effects like vortex induced vibrations and scour may occur. However, currents are generally quite localized and predictable and therefore easily avoidable. For workability analyses of cable pull-in operations dynamic current effects are normally not of great importance. Therefore it will not be considered further here.

Wind is a large energy source at sea. While this warrants the construction of the wind farms that require the installation of the submarine cables considered here, it also induces loads on everything that is exposed to it. As is the case for the current loading, any loads exerted on vessels and structures where station keeping

is important will need to be transferred by mooring lines or dynamic positioning systems. Furthermore, wind can be a highly variable phenomenon and wind gusts can induce significant dynamic loads on any system subjected to it. However, wind loading is normally not considered in the analysis of workability (DNV-GL, 2014) as the waves that are associated with any significant wind speeds would have rendered the situation unworkable first.

Waves are the primary motion and load generating influence at sea. The most important contributions to these waves are generated by the wind, either locally (wind-sea) or off-site (swell). When the wind has died down after wave generation and provided that the waves occur in sufficiently deep water and do not have too steep fronts, linear wave theory (Airy waves) describes the wave motions accurately. The following assumptions are made to be able to apply linear wave theory and are justified for the oceanic waves in the wave length ranges considered (Holthuijsen, 2007, p. 108-109):

- Ideal fluid**     The fluid is assumed to be incompressible, with constant density and zero viscosity.
- Continuous**     The body of water is continuous. In practice this means the water must contain no air bubbles.
- Gravity forced**     The only external forcing is provided by gravity.

The surface elevation of a propagating harmonic Airy wave is described as follows:

$$\eta(x, t) = \zeta \cos(kx - \omega t) \quad (3.1)$$

where the radial frequency and the wave number are related through the dispersion relation given as:

$$\omega^2 = gk \tanh(kd) \quad (3.2)$$

From the superposition of a large number of these linear harmonic waves over a range of directions and frequencies, a complete picture of an irregular sea state can be obtained through the following (Holthuijsen, 2007, p. 44-45):

$$\eta(x, y, t) = \sum_{i=1}^N \sum_{j=1}^M \zeta_{i,j} \cos(\omega t - k_i x \cos(\theta_j) - k_i y \sin(\theta_j) + \alpha_{i,j}) \quad (3.3)$$

For equations (3.1), (3.2) and (3.3) it holds that:

- |          |  |          |                            |
|----------|--|----------|----------------------------|
| $\eta$   | = Surface elevation [m]                          | $\theta$ | = Wave direction angle [°] |
| $\zeta$  | = Wave amplitude [m]                             | $\alpha$ | = Phase angle [rad]        |
| $k$      | = Wave number [rad/m]                            | $j$      | = Directional index [-]    |
| $\omega$ | = Radial frequency [rad/s]                       | $i$      | = Frequency index [-]      |
| $g$      | = Gravitational acceleration [m/s <sup>2</sup> ] | $d$      | = Water depth [m]          |

The combination of these individual components can be expressed in terms of an energy density spectrum, see Figure 3.10. The spectrum indicates how the energy in a sea state is distributed over frequencies (or wave numbers) and directions.

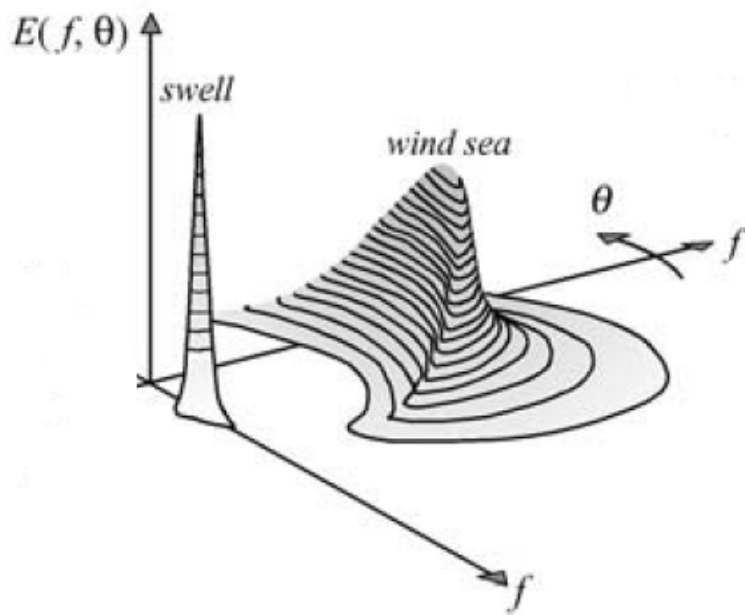


**Figure 3.10.:** Variance density spectrum of an irregular sea state incorporating a narrow swell peak and a widely spread wind-sea peak, taken from (Holthuijsen, 2007, p. 48).

” Those who cannot remember the past are condemned to repeat it.

— George Santayana

### 4.1 Offshore lifting by floating cranes

The operation of lifting a payload by means of a floating crane has been subject of much research for many different configurations. The quadrant with the cable suspended on it will start suspended in air, cross the splash zone and be submerged at different depths. These configurations are discussed here.

**Heavy payload suspended in air** Lifting a payload such as a quadrant in air with a crane on a floating vessel can be modeled using multi-body dynamics. The vessel subject to wave excitation is a six degree of freedom (DOF) system. Three translations: surge, sway, heave and three rotations: roll, pitch and yaw. The suspended payload exhibits the same motions bringing the total amount of degrees of freedom to twelve, as depicted in Figure 4.1.

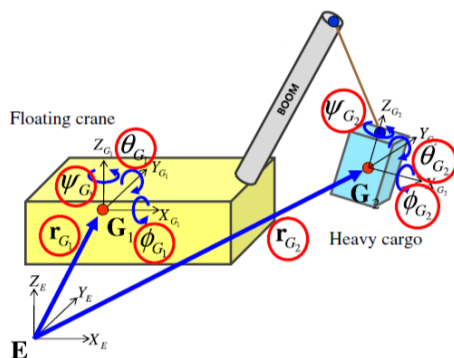


Figure 4.1.: 12 DOF crane-cargo system (taken from Cha et al. 2010)

Type of body	Reference area $S$ ( $b = \text{length}$ )	Reynolds number $Re$	Drag coefficient $C_D$	
Square rod		$S = b D$	$Re > 10^4$	$\rightarrow 2.00$
		$S = b D$	$Re > 10^4$	$\rightarrow 1.50$
Semicircular shell		$S = b D$	$Re > 10^4$	$\rightarrow 1.20$ $\leftarrow 2.30$
		$S = b D$	$Re > 10^4$	$\rightarrow 1.15$ $\leftarrow 2.15$
Equilateral triangle cylinder		$S = b D$	$Re > 10^4$	$\rightarrow 1.40$ $\leftarrow 2.10$
		$S = b D$	$Re > 10^4$	$\rightarrow 1.90$
T-beam		$S = b D$	$Re > 10^4$	$\rightarrow 1.80$ $\leftarrow 1.65$
		$S = b D$	$Re > 10^4$	$\rightarrow 2.05$
Hexagon		$S = b D$	$Re > 10^4$	$\rightarrow 1.00$
		$S = b D$	$Re > 10^4$	$\rightarrow 0.70$
Circular cylinder		$S = b D$	$Re > 10^4$	$\rightarrow 0.51$

Figure 4.2.: Drag coefficients for linear elements.

The lift wire couples the motions of the two bodies, making the motions and loads of one body dependent on those of the other and vice versa (Cha et al., 2010). Through this coupling the payload is excited by the external forcing on the vessel. Modelling the payload as a 6 DOF rigid body instead of a 3 DOF particle yields a larger and

more realistic motion behaviour for predominantly the roll motion of the vessel for heavy payloads. In the case where the mass of the payload is much smaller than the mass of the vessel, the influence of the payload on the motions of the vessel are negligible and the coupling can be eliminated. In this case the vessel is excited by the external forces only, and the vessel motions can be imposed directly on the payload suspension point.

**Submerged payload** With the payload submerged the dynamics change significantly. The payload will perform pendulum motions as a response to direct hydrodynamic loading in addition to the vessel induced motions. This pendulum motion is present for a single suspended payload in submerged conditions. However the presence of the vessel introduces a host of nonlinear hydrodynamic interaction effects that influence the motion response of the payload (Hannan and Bai, 2015). The natural frequency of the payload changes when submerged with respect to the in-air situation:

$$\omega_0 = \sqrt{\frac{(m - \rho_w * V) * g}{(m + m_a)L}} \quad (4.1)$$

- |            |  |     |                       |
|------------|--|-----|-----------------------|
| $\omega_0$ | = Payload natural frequency [rad/s]      | $m$ | = Mass [kg]           |
| $g$        | = Gravitational acceleration [ $m/s^2$ ] | $V$ | = Volume [ $m^3$ ]    |
| $m_a$      | = Added mass [kg]                        | $L$ | = Pendulum length [m] |
| $\rho_w$   | = Density of sea water [ $kg/m^3$ ]      |     |                       |

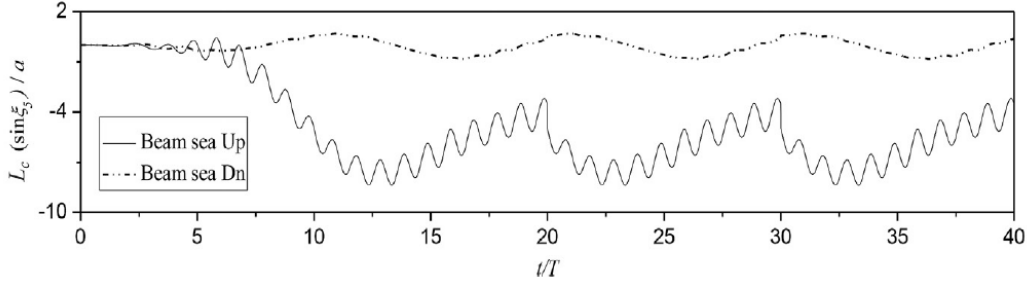


**Figure 4.3.:** Horizontal motions of payload in the presence of a fixed crane vessel. The low frequency component for the case of upstream beam loading is the natural frequency contribution, the high frequency component is the wave frequency and the negative mean signifies the mean drift force as a result of the interaction between the payload and the vessel. Picture taken from Hannan and Bai 2015.

Regardless of the excitation frequency of the waves, this natural frequency dominates the motion response of the heavy payload (Hannan and Bai, 2015). In this consideration it is assumed that the payload is the only body present in the water. Incorporating the presence of the crane vessel introduces nonlinear interaction effects between the vessel and the payload, even under the assumption of a fixed vessel. A shielding effect is observed in simulations where the oscillatory motion at the wave frequency is filtered out by the presence of the floating vessel in all wave directions. However, an increase in mean drift force is present with respect to the no-vessel case, as indicated in Figure 4.3.

**Splash zone dynamics** In the absence of current loading, excitation originates solely from waves. As wave energy decays quickly with depth, the hydrodynamic excitation is largest in the vicinity of the free surface: the splash zone. In this splash zone the air-water interface may also introduce slamming loads on the body transitioning from one medium to the other. The inline dynamic loads on a submerged body subjected to uniform oscillatory flow, in the direction of the flow, is approximated by the Morison equation:

$$F = F_I + F_D = \rho C_I V \ddot{u}_r + \frac{1}{2} \rho C_D A u_r |u_r| \quad (4.2)$$

$F_I$	= Inertia force [N]	$u_r$	= Relative velocity [m/s]
$F_D$	= Drag force [N]	$\rho$	= Density [kg/m <sup>3</sup> ]
$C_I$	= Inertia coefficient [–]	$V$	= Volume [m <sup>3</sup> ]
$C_D$	= Drag coefficient [–]	$A$	= Area perpendicular to flow [m <sup>2</sup> ]

The first term represents the inertia effect which is in phase with the relative acceleration. It accounts for the mass of the body and the added mass mobilized by the motion. The second term represents the drag effect which is out of phase with the inertia contribution. The force normal to the flow direction is not included in this formula. This lift force has to be determined separately.

The coefficients in (4.2) are dependent on the Reynolds number, Keulegan-Carpenter number and surface roughness and generally need to be determined experimentally. For regular shapes such as cylinders, spheres and plates the coefficients are known and given in Figure 4.2.

For payloads of irregular geometry these coefficients are not readily available. Instead they need to be approximated or determined experimentally. The most commonly used method is to divide the structure into regularly shaped components for which the coefficients are known. The total added mass and drag contribution is then assumed to be a summation of the individual components. For structures consisting of flat surfaces the coefficients are determined by adapting the situation of a flat plate perpendicular to the flow to a situation of body depth, see Figure 4.4. A reduction factor is applied for perforated surfaces in the form of  $\exp(-P/28)$  where P is the perforation ratio (Sarkar and Gudmestad, 2010).

In the splash zone the flow can no longer be assumed to be steady. This means that the hydrodynamic coefficients valid for steady flow do not apply. In lifting analyses it is suggested to apply a factor 2 to the drag coefficient. Caution is necessary here, as for inertia dominated situations this may introduce unrealistically high damping values. In addition to this, the proximity of the object to the free surface has an effect on the added mass of the system. The absence of water above the object reduces the added mass. This effect is primarily observable in heave direction as the added mass is in this case mostly mobilized above and below the object. For tubular elements, fully developed added mass must be assumed from a water column above the object of twice the radius or more. Below this a reduction may be applied as illustrated in Figure 4.5.

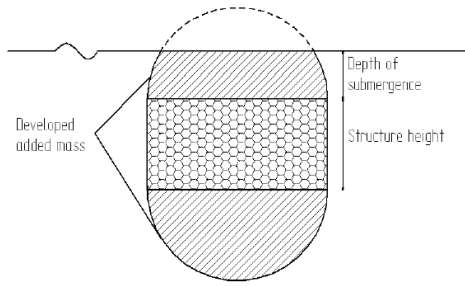


**Figure 4.4.:** Added mass for a flat object near the free surface as suggested by Sarkar and Gudmestad 2010.

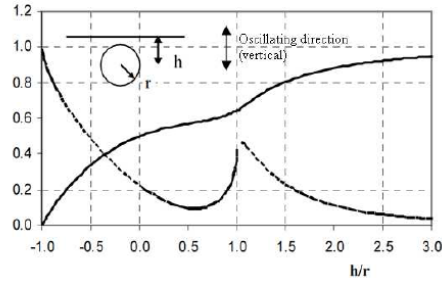


**Figure 4.5.:** Normalized added mass of a cylinder near the free surface (solid line) and the normalized rate of change (dotted line), illustration taken from: Sarkar and Gudmestad 2010.

## 4.2 Catenary mooring systems

The configuration that a cable assumes when being pulled in and being supported by a quadrant resembles a catenary mooring line. Given the fact that they have been around for a long time, research into the dynamic behavior of catenary mooring lines is available.

**Static catenary** In order to provide the dynamic analysis with an equilibrium condition an assessment can be made of the configuration of the cable in a static situation. The simplest configuration is that of a cable suspended on two suspension points loaded by gravity alone. The shape the cable assumes in this state is a catenary (see Figure 4.6), described analytically by the catenary equation:

$$y(x) = a \cosh(x/a) \quad \text{with : } a = T_0/wg \quad (4.3)$$

$a$	= Catenary parameter [m]	$w$	= Submerged cable weight [kg/m]
$T_0$	= Bottom tension force [N]	$g$	= Gravitational acceleration [m/s <sup>2</sup> ]
$x$	= X coordinate [m]	$y$	= Y coordinate [m]

For a cable with given properties the catenary is fully described by the bottom tension and the horizontal coordinates of the suspension points. From horizontal static equilibrium it follows that the horizontal component of the tension in the line is a constant for each position in the line, equal to the bottom tension  $T_0$  in the case where one end rests on the horizontal seabed. Given the cable weight, the tension in the axial direction of the cable and the arc length can be determined as:

$$T(x) = \frac{T_0}{\cos(\alpha(x))} = \frac{T_0}{\cos(\arctan(dy/dx))} \quad (4.4)$$

$$l(x) = a \sinh(x/a) \quad (4.5)$$

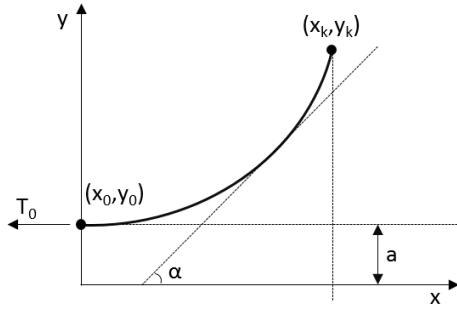


Figure 4.6.: Catenary graph

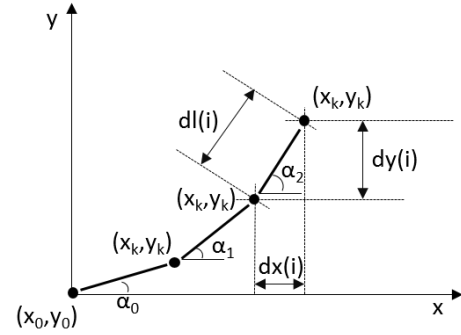


Figure 4.7.: Discretization

To be able to analyse the system it is necessary to discretise the problem. This is done by dividing the cable into  $N$  segments of equal length  $dl = \frac{l}{N}$  and  $k = N + 1$  nodes. The angle of the cable segment with respect to level is determined as  $\arctan(\frac{dy}{dx})$  as specified in Figure 4.7. Using this in combination with equation 4.4 the tension in the considered cable segment is determined if the node positions are known.

**Catenary dynamics** The basis of analyzing the catenary mooring line dynamics is provided by the Lumped Mass Method (Walton and Polachek, 1960; Nakajima et al., 1982; Van den Boom, 1985). It consists of a discretization of the line such as presented in Figure 4.7. In this discretization all forces and masses are concentrated (lumped) in the nodes. These nodes are connected by massless linear springs that provide tension interaction between the nodes. An equation of motion can be formulated for the mass of each node  $i$  in both vertical and horizontal direction:

$$\left( \begin{bmatrix} M & 0 \\ 0 & M \end{bmatrix}_i + [m_a(t)]_i \right) \begin{bmatrix} \ddot{x}(t) \\ \ddot{z}(t) \end{bmatrix}_i = \begin{bmatrix} F_x(t) \\ F_z(t) \end{bmatrix}_i \quad (4.6)$$

For which the added mass matrix is given by equations 4.7 to 4.9. The force components  $F_x(t)$  and  $F_y(t)$  on each node are presented in equation 4.10 and consist of weight and buoyancy, cable tension in the adjoining sections and hydrodynamic drag (Section 7.2 and Appendix B). In addition to this there is interaction between cable and quadrant near the top and between cable and soil on the seabed.

$$[m_a]_i = a_{n,i} \begin{bmatrix} \sin^2 \theta_i & -\sin \theta_i \cos \theta_i \\ -\sin \theta_i \cos \theta_i & \cos^2 \theta_i \end{bmatrix}_i + a_{t,i} \begin{bmatrix} \cos^2 \theta_i & \sin \theta_i \cos \theta_i \\ \sin \theta_i \cos \theta_i & \sin^2 \theta_i \end{bmatrix}_i \quad (4.7)$$

$$a_{n,i} = \frac{\pi}{4} \rho C_{I,n} D_i l_i \quad \text{and} \quad a_{t,i} = \frac{\pi}{4} \rho C_{I,t} D_i l_i \quad (4.8)$$

$$\theta = \alpha_i + \alpha_{i-1} \quad (4.9)$$

$$\begin{bmatrix} F_x(t) \\ F_z(t) \end{bmatrix}_i = \underline{F}_i = \underline{F}_W + \underline{F}_B + \underline{F}_D + \underline{F}_S + \underline{F}_Q + \underline{T}_i - \underline{T}_{i-1} \quad (4.10)$$

$m$	= Mass [ $kg$ ]	$l$	= Segment length [ $m$ ]
$m_a$	= Added mass [ $kg$ ]	$\alpha$	= Segment angle [deg]
$t$	= Time [ $s$ ]	$\rho_w$	= Density of sea water [ $kg/m^3$ ]
$x$	= X coordinate [ $m$ ]	$C_I$	= Inertia coefficient [–]
$z$	= Z coordinate [ $m$ ]	$D$	= Diameter [ $m$ ]
$\theta$	= Average node angle [deg]	$T_i$	= Tension in segment i [ $N$ ]
$a_n$	= Normal added mass [ $kg$ ]	$i$	= Node and segment index
$a_t$	= Tangential added mass [ $kg$ ]		

For each time step in the dynamic analysis a Newton-Raphson solver will iteratively find a stable configuration of the cable. The input for the Newton-Raphson solver is a configuration of the cable that is not too far away from the solution. For the initial condition the analytic catenary equation provides this configuration. For each new time step the solution of the previous time step is used as an initial condition. This is with the exception of the top node, which is subject to the imposed motion.

The Newton-Raphson iterator will find a converged solution of the configuration for each time step. The excitation of the top end, the environmental loading from the previous time step and the configuration of the previous time step (static configuration for the first time step) provide the input conditions. The iterator will determine the node positions first, then determine the forces in the line as a result of the node positions, increment the positions of the nodes as a result of the forces and repeat the process until a specified convergence is achieved.

### 4.3 Cable failure modes

Submarine cables constitute a vulnerable element in offshore wind farm systems. Numerous ways exist in which submarine cables may potentially fail, each of which is activated in different stages of life and by varying conditions. While the cables main purpose is to transmit power, electrical influences may affect cable performance. With high voltages and currents present in the cable in combination with the multitude of components comprising the cable, electrical interaction effects can instigate failures such as overheating or even arcing between cable elements (Coates, 2018).

Over the course of time the materials that make up the cable will start to degrade. Each individual layer is, or may become, exposed to electrical loading, abrasive environments, marine growth or water ingress. This in turn can lead to a host of material degradation effects like corrosion, erosion, water treeing, layer separation and other long term exposure effects that impair the cables current carrying capacity (Worzyk, 2009).

While these failure mechanisms need to be taken into account in cable design and routing, they are of minimal importance for the cable installation process. The failure modes induced by mechanical loads are the main factors limiting operability and workability.

**Tension & compression** During the pull-in operation the cable is subjected to a range of tension forces. Correct application of tension can prevent a lot of failure modes in the cable and therefore a certain tension is desired in many stages of installation. However, overtension can also damage a cable. The armor wires will assume the applied load and tighten around the core due to its helical structure. This has the potential to damage insulation layers and metallic sheathing around the conducting cores.

Compression in the cable is generally undesirable. Compression loads may cause buckling of cable components such as sheathing. It can also induce a phenomenon in the armor wires known as birdcaging: unwinding of the armor wires due to the helical structure in response to compression, as displayed in Figure 4.8.

Manufacturers of cables circumvented these failure modes by specifying zero compression capability for the cables in the past, straining cable installers extra in heavy conditions. Recently, more research into cable compression is performed causing this stringent limit to be relaxed to some extent.

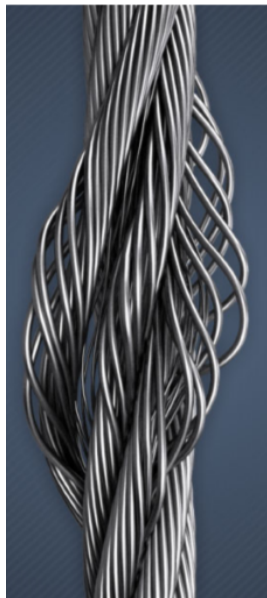


**Figure 4.8.:** Bird-caging.

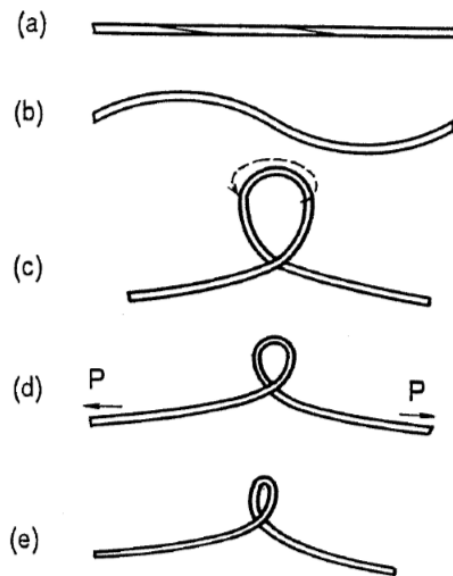


**Figure 4.9.:** Cable kink formation process, taken from (Yabuta, 1984).

**Overbending** The different components that make up the submarine HVAC cables respond differently when the cable is flexurally loaded. This is dictated first of all by the different properties of each component. Secondly, the bending load generates a region of tension on one side of the cable and one of compression on the other, leading to different responses. When bending the cable, at first the response is elastic. In the tensionally loaded region the components strain positively and in the compressive region the components strain negatively. When the bending load is released the cable will return to its equilibrium state without permanent deformation. The individual components will also show different strain behavior with respect to each other in equal loading conditions. When loading the cable in bending beyond

a certain threshold, these different strains will overcome the frictional resistance between the components and induce slipping of components. With the relatively high static friction between components now overcome, the overall bending stiffness will reduce, as shown in Figure 3.8. If the bending radius is even further reduced to below the specified MBR, the relative movement of the components and the severe strain on them will damage the integrity of the cable. The individual armoring wires start unwinding, resulting in birdcaging. Other effects that may occur include deterioration of electrical insulation and buckling of sheathing, which in turn can lead to water ingress.

Assuming that storage and handling of the cable prior to the installation effort is done properly, exceedance of the MBR during pull-in operations can occur at the hang off point in the chute, at the touch down point on the bottom or at the hang off points on the quadrant. Even though the quadrant is used to maintain acceptable bending radii, the use of rollers may incidentally cause overbending in high tension scenarios (BPP Cables, 2017).

**Torsion, loop formation & cable kinking** Torsion will occur in the cables as a result of the helical structure of the armoring wires. During the laying process the cable will experience a certain tension, which is converted to a torsional load through the helical wiring. Other sources of torsion include residual twist of the cable from loading and paying out the cable on and off the carousel. A torsion load is not a problem as long as the cable is properly tensioned. However, when a significant twist is present in the cable in situations where tension is low or compression is present, the cable will start to deform. First the cable will assume a helical shape. If this is not resolved by restoring tension on the cable or reducing cable twist, a loop may form, absorbing one rotation of the cable. In itself this is not an issue as long as the MBR limit is not exceeded. However, when tension is restored on a looped cable the loop decreases in diameter and may kink (see Figure 4.9), damaging the cable in the process (Yabuta, 1984).

**Crushing & squeezing** A cable faces radial compressive loading even before the final installation effort. In the carousel that holds the cable on the CLV the cable is coiled vertically. The sections of cable that lie on the bottom carry the weight of the rest of the cable on top. With a total loading capacity of 4600 ton of cable, these squeezing loads can become quite large.

During installation of the cable and during its design life time the cable is loaded in crushing in several ways. Rocks, anchors, dropped objects and tensioning grippers all exert crushing loads. Another regularly implemented limit is the maximum side-wall pressure (SWP) (Worzyk, 2009). This unit describes a force per unit length and can be defined as:

$$SWP = F_t/R \quad (4.11)$$

Where  $F_t$  is the tension force on the cable and  $R$  is the radius. The side-wall pressure (SWP) is a measure of the lateral squeezing load the cable can incur. Especially while handling the cable on the quadrant this is a factor as the bending radius will be close

to the minimum there while tension can not be released by cable movement. Exceeding the maximum crushing load may damage the internal components. It can also reduce resistance to other external loads and influence the fatigue lifetime of the cable (Guttner et al., [2017](#)).



## Current analysis methodology

” *Any company that embraces the status quo as an operating principle is on death march.*

— **Howard Schultz**  
(former CEO Starbucks)

As the motion behavior of the quadrant and the cable in reaction to wave loading on the CLV is highly nonlinear during the second end pull-in operation, the current analysis methodology relies on simulating the problem in all complexity. The nonlinearity of the problem requires the simulations to be executed in the time domain as opposed to the much less computationally expensive frequency domain. As the workability for the operation may be subject to a large set of conditions the amount of simulations that must be executed is high. After simulating the problem for all cases an assessment is made into which conditions are suitable for the operation to take place in.

### 5.1 Simulation steps

While being a small part in the overall cable laying operation, the second end pull-in operation itself consists of several stages as shown in figures 3.1-3.5 in section 3.1. For the analysis of the workability it is convenient to assess these stages separately. Stages 1 and 2 are typically not critical and can be modeled similar to normal cable lay as the cable hangs of the chute normally. For snapshots 3-5 the quadrant makes the problem more complex, which requires the need for extensive simulations. For each of these snapshots a separate Orcaflex model is created. This model consists of the CLV including response amplitude operators (RAOs), the quadrant made up of Morison elements, the crane wire, the cable and the environmental data. For each model and each load case a 10 hour time trace is generated of the crane tip motions. This is done by generating a wave train from the spectral input data of the waves and applying the RAOs on this time trace. The influence of the cable and the quadrant on the ship motions are negligible given the mass differences between the two. This means that the ship motions may be determined without simulating the computationally intensive cable and quadrant. Subsequently, the crane tip motions may be imposed on the crane wire for the full system, applying the wave train as well to account for direct wave loading of the cable and quadrant. Running a full 10 hour simulation for all load cases in all the snapshots would require too much computing power. Therefore, a reduction is applied in the time

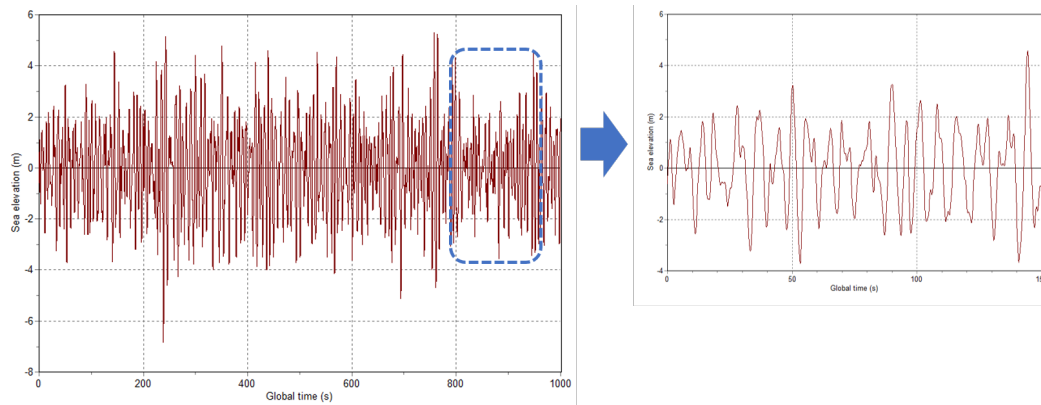


**Figure 5.1.:** Reduction of the wave time trace from a long record to 150 seconds around the highest rise or fall velocity. This time trace is then applied to the full model including the cable and quadrant to keep computational intensity manageable.

traces that decreases the amount of required calculations. To do this, in each time trace of the crane tip motion, the moments of highest rise and highest fall velocity are determined. A time trace of 150 seconds of the environment and the crane tip motion around these moments is taken from the total record, as displayed in Figure 5.1. These time traces are then applied to the suspended cable-quadrant system and the motions are simulated after which the results need to be interpreted.

## 5.2 Modeling of cables

The most important element of the model is the cable. The cable is modeled according to the lumped mass method (LMM). It is divided into a number of nodes, as shown in Figure 5.2, where all the forces and masses of the surrounding segment of cable is concentrated, connected by linear springs. The method was originally developed to analyse the dynamic behavior of catenary mooring systems. It incorporates the self weight in water of the cable, drag and inertia influences and axial stiffness of the cable.

For mooring systems this is enough to model the dynamic behavior. For cable modeling however, this is not sufficient. Besides axial stiffness the cable also resists bending motions and rotational motions. This is incorporated by introducing bending springs in the respective direction of the motion considered (Figure 5.3). Determining the stiffness of these springs is not straightforward. Due to the inhomogeneity of the cable structure, the magnitudes of the stiffness is often nonlinear and motion dependent. Furthermore, there are several interdependencies between loading in one direction and stiffness variations for another degree of freedom. This is for instance the case for the rotational stiffness under axial tension. The helical structure of the armor wires (section 3.2) tightens around the core and increases rotational stiffness. A difference in rotational stiffness is also observed for clockwise and counterclockwise rotation, as this either opens or tightens the helical winding.

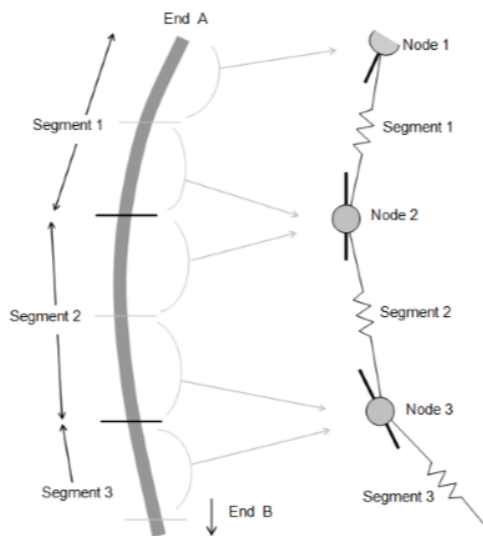


**Figure 5.2.:** LMM discretisation (taken from *Orcaflex user manual*).

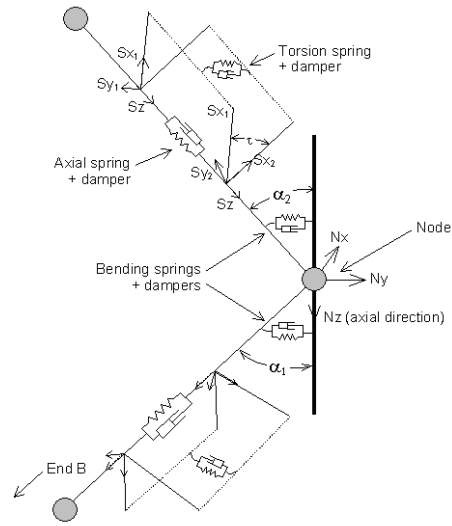


**Figure 5.3.:** Full LMM method as used by Orcaflex (taken from *Orcaflex user manual*).

Special attention is required in correctly implementing the bending stiffness of the cable. It has a profound effect in the reaction of the cable and the stiffness itself depends non-linearly on the curvature. In some cases a stiffness curve is provided by the manufacturer that quantifies the cable bend stiffness at different curvatures.

Damping in the model can be applied by introducing dampers next to the springs. Hydrodynamic drag is a source of damping as well as bending hysteresis, which can be implemented if a hysteresis loop is available for the cable. Seabed damping is not incorporated due to the calculation method, which is further elaborated in Section 5.4. For several instances however, the damping ratio is difficult to determine. This is overcome by introducing Rayleigh damping to the system of a small fraction of the critical damping ratio.

### 5.3 Environmental loading

The environmental effects that are incorporated in the analysis are the seabed interaction, wave effects and, in some cases, current. The current is modeled as a constant flow in time and in space. The seabed can be modeled in two ways: as an elastic or a viscoelastic solid. As the viscoelastic solid seabed accounts for damping in the interaction between cable and soil, better operability values are expected than for the purely elastic seabed interaction. However, modeling the seabed viscoelastically limits the choice in calculation methods (see section 5.4). For this reason the soil is modeled as an elastic solid and the damping is neglected.

The most important environmental effect is the contribution of waves. The waves excite the quadrant and the cable directly as well as through the vessel. As described in section 3.5, the wave system is characterized by a spectral representation. It is determined by the superposition of linear harmonic wave components. Each of

the components is in turn described in terms of the  $H_s$ ,  $T_p$  and direction. These parameters are discretely defined to limit the possible combinations and therefore the number of calculations. The  $H_s$  is defined in increments of 0.25 meter, generally up to 2.5 meters. The  $T_p$  is either derived from the value of  $H_s$  using a  $\gamma$  value, or incremented by 1 second if a full matrix is desired. The wave incidence angles are varied by increments of  $22.5^\circ$  over the full range of directions, in order to account for asymmetries.

## 5.4 Calculation method

In order to calculate the motions and loads of the system, for each node an equation of motion can be formulated in the form of an ordinary differential equation. These equations are then solved using an implicit time integration scheme with constant time step. This generalized- $\alpha$  method determines the forces on each node and solves equations of motions at the end of each time step. The downside of this implicit method is that it requires an iterative process to determine the solution, increasing calculation times per time step. However, contrary to explicit schemes, the implicit method is unconditionally stable for every time step size. This means that larger time steps can be used and therefore fewer calculations are required, making the implicit method significantly faster. A downside of the implicit integration is that the model does not allow for seabed damping.

## 5.5 Workability assessment

The limiting mechanical cable load parameters are extracted from the analysis results. These include the maximum tension as well as compression in the line, the MBR, the SWP (equation 4.11) and the contact load. If any of these occurring loads exceeds the specified maximum of the cable, the case is deemed failed and the situation is flagged as inoperable. Combining all the simulated cases provides an envelope of sea states in which the operation can be performed without exceeding the cable limits. This operability envelope is visualized in a rose plot of which an example is provided in Figure 5.4. Comparing these limits with statistical weather data of a work location for a specified time of the year, the workability of the activity can be expressed as a percentage of time in which the activity can be expected to be safely performed.

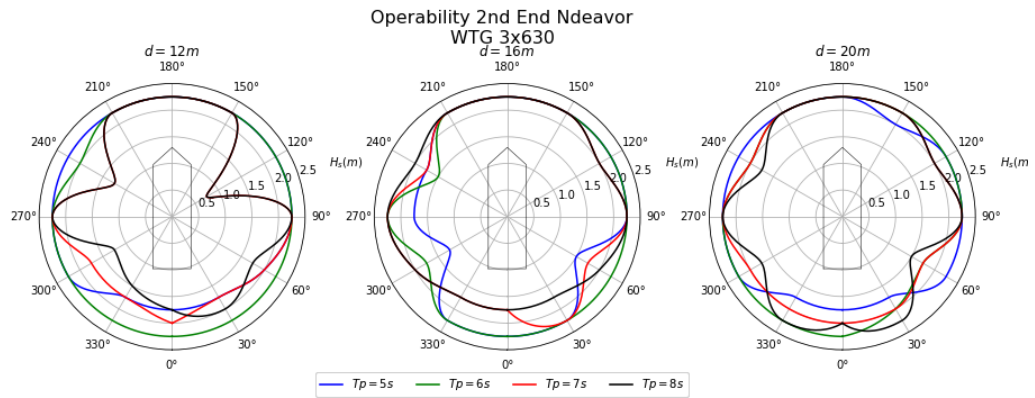


**Figure 5.4.:** Example operability plot for a second end pull-in operation depicting operable  $H_s$ ,  $T_p$  and direction combinations for a given vessel and water depth  $d$ .

## 5.6 Method improvement

While the current assessment method provides a means to quantify the operability and workability of the pull-in operation, and other operations alike, it does include some caveats. First of all, the calculations in the time domain take a lot of processing power. The implementation of vessel motion limits would allow for the elimination of the time domain simulation for each load case. Instead, the ship motions can be determined in the frequency domain using RAOs, from which it can be determined if the limits are exceeded, greatly reducing calculation times. Furthermore, the sea state limits are presented in tables of all the possible combinations of  $H_s$ ,  $T_p$  and direction. Comparing these discretized sea state limits with sea state forecasts can cause some situations close to the limit to be flagged as inoperable while in reality they are not. This discretization error can be removed if a vessel motion limit can be formulated, which eliminates the need for discretization in the limits.



” *No plan survives contact with the enemy.*

— **Helmuth von Moltke**  
(Prussian general)

## 6.1 Modeling and analysis process

The first step in analyzing the problem is to determine which stages of the process are critical regarding cable integrity. The second end pull-in process is described in chapter 3. Some of the snapshots represent minor loading conditions or resemble the continuous cable laying process making it unnecessary to include it in this analysis. The relevant snapshots that will be analyzed are then modeled in Orcaflex in order to apply the necessary motions to the system. This is described in more detail in chapter 7.

The next steps are schematized in Figure 6.1. First the environmental situations that excite the system are established. In order to do this a vessel is selected and based on the vessel properties a set of extreme sea states is determined in which the vessel may reasonably be expected to operate. Once the sea states and the model are implemented to satisfaction, the sea states are applied to the vessel model to find the vessel motions for each specific load case. From the vessel properties and the location of the suspension point on the vessel, the motions of said suspension point can be determined. Once the suspension point motion is known, it can in turn be imposed on the suspended cable-quadrant model. The system will now move according to the implemented effects and the cable will be subject to forces and changes in geometry. These mechanical cable properties are recorded along with the motions of the suspension point and quadrant. This data set is then visualized

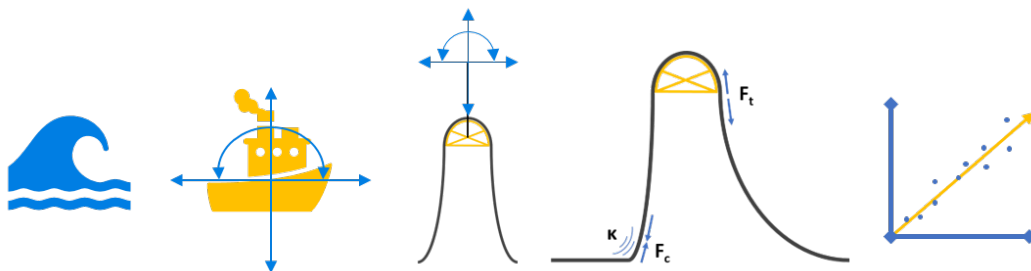


**Figure 6.1.:** Analysis process schematization: sea state determination, vessel motion analysis, suspension point motion, cable response, curve fitting and limit statements.

in graphs in order to determine relations between input and output parameters. The final task is to formulate limits to the input motions for which cable integrity is maintained.

## 6.2 Configuration

The pull-in process is divided into stages that may potentially be critical regarding cable integrity. These 'snapshots' are modeled and analyzed separately to assess the different system configurations, loading conditions, motion responses and governing limit states accurately. The general configuration, loading and motion components are depicted in Figure 6.2. The system is excited by a motion of the crane tip, which in turn is generated by the vessel response to the sea state. Under influence of this motion the quadrant may perform pendulum motions. The sea state also directly loads the quadrant and the cable.

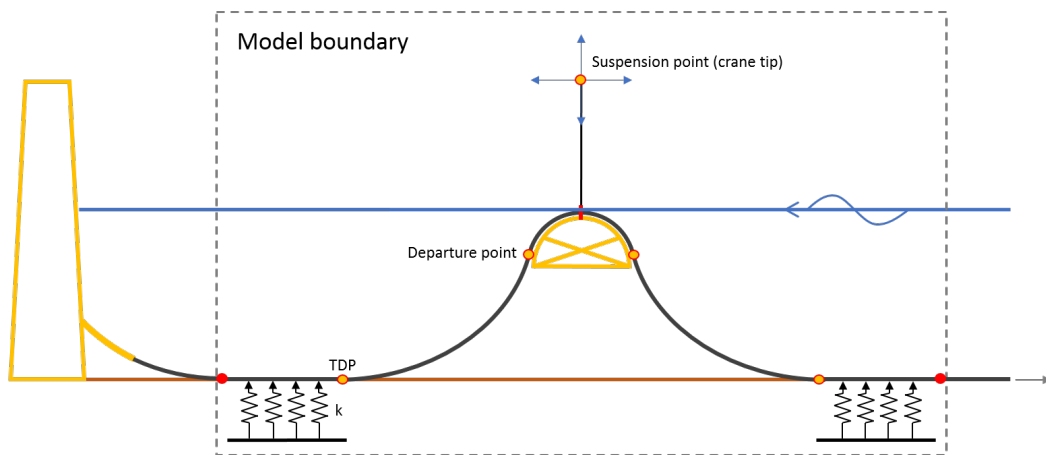


**Figure 6.2.:** General static configuration of the cable-quadrant system suspended on the vessel crane tip. In the dynamic analysis it is subject to direct sea state loading on the quadrant and the cable, as well as to crane tip motion (as generated by the vessel motions which in turn are generated by the sea state).

The configuration displayed in Figure 6.2 is assessed in various stages of the installation process: the snapshots discussed in Section 3.1. Snapshots A and B from Figure 3.1 and 3.2 are similar to the continuous cable laying process as the cable hangs off the chute on the stern of the vessel and will therefore not be investigated further. Snapshots C to E (Figure 3.3-3.5) are investigated as they represent potentially critical configurations with separate loading and motion behavior characteristics. These snapshot are from here on out labeled as 1,2 and 3, as displayed in Figure 6.3:

**Snapshot 1: in-air** In this snapshot the quadrant is hanging in the air by a crane wire, free to perform pendulum motions under influence of the crane tip motion. The cable catenaries will influence this motion. Direct wave loading occurs on the submerged part of the cable. No hydrodynamic interaction takes place on the quadrant. This means the system damp-

ing is relatively low, and motions can potentially become relatively large. This snapshot therefore has the potential to become a limiting factor in the operation.

**Snapshot 2: splash zone** In snapshot 2 the quadrant is just fully submerged. Hydrodynamic loading occurs on the quadrant and the entire cable. The higher drag on the system this introduces, dampens the motion amplitude. However, maximal direct wave loading occurs on the quadrant and the cable, as wave motion is most severe near the surface. This means that snapshot 2 is also potentially limiting.

**Snapshot 3: near seabed** Near the end of the operation the quadrant is located close to the seabed. The hydrodynamic interaction damps motion and the direct wave loading is minimal due to the influence decaying with depth. The quadrant motions will therefore be smaller than in snapshots 1 and 2. However, the geometry of snapshot 3 is less favorable. Virtually no catenaries are present in the cable to absorb quadrant motions. Relatively small motions may therefore have amplified effects in the cable response. For this reason, an analysis of snapshot 3 is warranted as well.

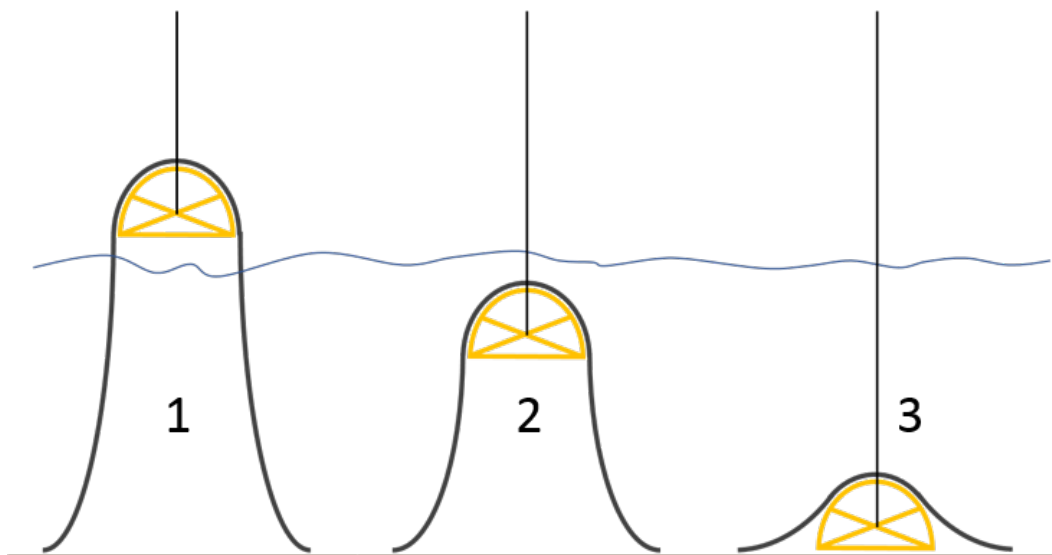


**Figure 6.3.:** Three snapshots that are considered in this thesis: 1. The quadrant is suspended above the water; 2. The quadrant is situated just below the surface; 3. The quadrant is near the seabed.

## 6.3 Sea states

As a wide variety of sea states may occur while computation power is finite, a restriction in the number of sea states that is analyzed is required. Some sea states have parameter combinations that have a theoretical occurrence probability at best (area A in in Figure 6.4). These are discarded. In the remaining possibilities a range of sea states is beyond safe operating limits for the vessel regardless of cable failure and

can also be discarded (area B). Sea states that are so tranquil in nature that hardly any excitation is generated are not of interest and may also be discarded (area D). The sea states of interest are those that have a reasonable chance to occur, while generating the system responses close to the cable failure envelope (shaded area C). The sea states that are imposed on the vessel follow from a vessel motion analysis (VMA) of the Stemat Spirit CLV, this process is described in detail in Appendix A. The RAOs of the vessel are known from a diffraction model. These RAOs are used to determine the reaction of the vessel to sea state in a range of wave periods and wave heights. These are compared to a set of limits for which the vessel would abort operation for reasons other than cable integrity. These limits consider a maximum wave height (eq. 6.1), a roll angle limit (eq. 6.2) and a heave acceleration maximum (eq. 6.3):

$$H_s^{max} = 3.5 [m] \quad (6.1) \quad \zeta_{4,crit} = 8 [deg] \quad (6.2) \quad \ddot{\zeta}_{3,crit} = 3 [m/s^2] \quad (6.3)$$

For a set of wave periods the wave height is chosen that generates the maximum motion of the suspension point of the crane while the vessel motions remain below the limit. This is done for both maximum heave and sway response of the suspension point. The maximums represent values for JONSWAP spectral parameters  $T_p$  and  $H_s$ . However, the cases are also applied as airy waves with the same values for wave height and wave period. The cases are presented in Figure 6.5.

While this is a good estimate of the maximum sea states that may be encountered, it is still an incomplete set. However, this is not a problem, as the sea states are only auxiliary parameters. The input parameters of interest are the acceleration, velocity and displacement magnitudes of the suspension point. These follow from the reaction of the vessel to the sea states and will be related to the response data.

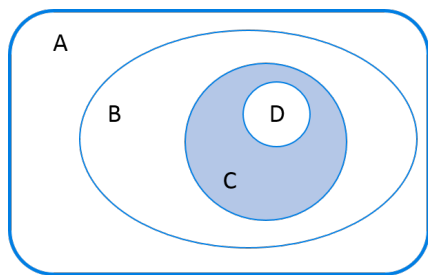


Figure 6.4.: Sea state selection diagram.

Tp [s]	Heave				Sway			
	case	$\zeta$ [m]	dir [°]	Hs [m]	case	$\zeta$ [m]	dir [°]	Hs [m]
5	1	2.40	75	3.35	8	1.80	105	3.50
7.5	2	3.91	-15	3.49	9	2.36	-135	3.02
10	3	5.16	45	3.46	10	3.66	-135	3.50
12.5	4	4.88	30	3.50	11	4.28	-60	3.50
15	5	4.63	30	3.50	12	4.79	60	3.50
17.5	6	4.37	30	3.50	13	5.25	60	3.50
20	7	4.15	15	3.50	14	5.72	75	3.50

Figure 6.5.: Load cases derived from the VMA.

## 6.4 Vessel response

With a set of sea states determined, they can be simulated and applied to the vessel. The vessel response to the sea state is determined by the RAOs, which are known for the vessel at specified draft and water depth. In contrast with the determination

of the load cases, the response is now determined in the form of a time trace. The motion of the crane tip is determined from the vessel response through geometry:

$$X_{ct} = l * \sin(\psi) - h * \sin(\chi) + \xi_{cog} \quad (6.4)$$

$$Z_{ct}(t) = l * \sin(\phi) + b * \sin(\chi) + \zeta_{cog} \quad (6.5)$$

$X_{ct}$	= X position of crane tip relative to CoG [m]	$\psi$	= Vessel yaw [deg]
$Z_{ct}$	= Z position of crane tip relative to CoG [m]	$\chi$	= Vessel roll [deg]
$l$	= length between crane tip and CoG [m]	$\phi$	= Vessel pitch [deg]
$h$	= height between crane tip and CoG [m]	$\xi$	= Vessel surge [m]
$b$	= width between crane tip and CoG [m]	$\zeta$	= Vessel heave [m]

The motions of the suspension point are the actual parameters of interest, as these can be applied to the cable-quadrant system, generating a response in the cable. The motions of the crane tip that are considered here are the displacement, velocity and acceleration in heave and sway directions (and axial; see Section 6.5 and Figure 6.6). Surge motion is not considered here in order to maintain a manageable amount of parameters in the complete analysis. The suspension point motion can then be related to the response in order to apply further analysis as described in Section 6.6. This process is carried out under the assumption that the vessel motion is not influenced by the loads applied by the cable-quadrant system to the vessel. This allows the vessel response to be determined separately from the response of the rest of the model. A calculation supporting this assumption is given in Appendix A.

## 6.5 Static and dynamic analysis

The configurations of section 6.2 are first assessed in the static state before any dynamic analysis is performed. The static loads in the cable and the geometry of the system under gravitational loading are used to normalize the results of the dynamic analyses. The maximum tension and maximum curvature are always positive quantities, which are therefore easily normalized by the maximum static values. Compression is not present in the line in the static situation and is therefore expressed as the maximum tension loss in the line normalized by the minimum tension present in the line in the static situation. This way, compression can be expressed as a positive dimensionless number for any conceivable state, much like tension and curvature.

$$\bar{T} = \frac{T_d^+}{T_s^+} \quad (6.6) \quad \bar{\kappa} = \frac{\kappa_d^+}{\kappa_s^+} \quad (6.7) \quad \bar{F}_c = \frac{T_s^- - T_d^-}{T_s^-} \quad (6.8)$$

In the dynamic analysis the suspension point motion is assessed in three directions and three quantities. The directions include vertical (heave) and horizontal (sway) motions and motions in the direction of the cable such as it is at the point of contact

- $\bar{T}$  = Normalized tension [-]
- $\bar{\kappa}$  = Normalized curvature [-]
- $\bar{F}_c$  = Normalized compression [-]
- $T_d^+$  = Max. dynamic tension [ $kN$ ]
- $T_s^+$  = Max. static tension [ $kN$ ]
- $\kappa_d^+$  = Max. dynamic curvature [ $1/m$ ]
- $\kappa_s^+$  = Max. static curvature [ $1/m$ ]
- $T_d^-$  = Min. dynamic tension [ $kN$ ]
- $T_s^-$  = Min. static tension [ $kN$ ]

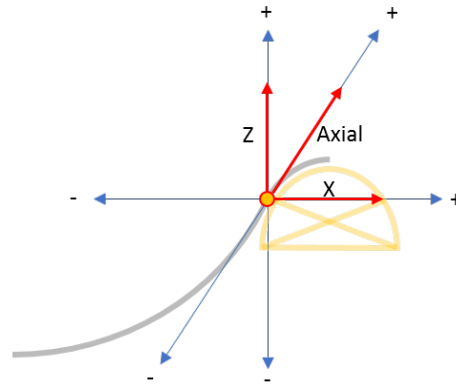


**Figure 6.6.:** Directional convention with the static configuration of the cable on the quadrant as a reference.

with the quadrant in the static situation, which is displayed in Figure 6.6. This axial direction of interest comes from the previous work of (Loos, 2017), who showed that for normal cable laying, top end motion in this direction is critical with respect to cable loads. For each direction a distinction is also made between the negative direction of motion and the positive, as this is anticipated to show different responses. The parameters of interest for the suspension point are the acceleration, the velocity and the displacement. These parameters, in each direction, are then related to the extreme responses of the cable in chapter 8.

The excitation of the suspension point through the vessel motion and the direct influence of the sea state on the cable-quadrant system will generate a response in the cable. For each simulation a complete time record is generated in each node of the tension (and compression) and the curvature. From this record the extremes values are determined, which are then used to identify the relations of interest.

## 6.6 Results

The results of the simulations are visualized in scatter plots. These display the full set of simulations per snapshot, relating one of the input parameters of the suspension point (displacement, velocity or acceleration) to an output parameter of the cable response (tension, compression or curvature). Each point in the plot represents a single simulation. The collection of the acquired data points are used to determine the relations between the input and output parameters. This is done by applying a polynomial regression through the data points. **This polynomial is linear in the coefficients and therefore represents a conversion of the data to a linear model.** The accuracy of the polynomial fit is determined by specifying an  $R^2$  score between 0 and 1, where a score closer to 1 indicates a better fit. The validity and applicability of the  $R^2$  score is verified by performing residual errors plots and F-tests on the fitted curves. A prediction interval is added to signify the uncertainty

range of predictions of the model. A more detailed description of the polynomial regression and the validation and verification steps is given in Appendix C. With the relations determined, they can be used to assess the mechanical response of the cable to suspension point motion parameters. Comparing the motion parameters to the mechanical cable limits, a statement can be made about limits to the suspension point motion. This allows the full problem to be analyzed in the frequency domain to obtain real-time results of any sea state encountered.

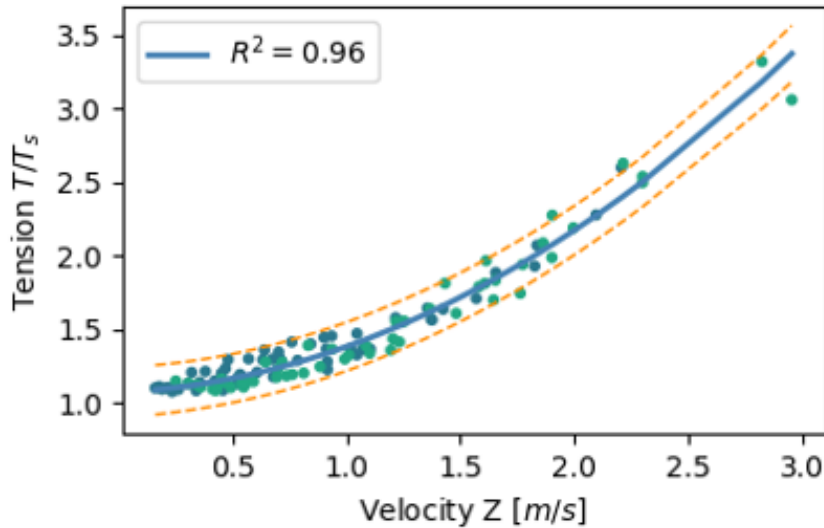


**Figure 6.7.:** Example of a scatter plot. It displays the normalized tension in relation to the heave velocity for snapshot 2. Plotted along with the data points are the fitted polynomial regression line labeled with a goodness of fit score, and a 95% prediction interval for new data points based on this data. The different colored data points indicate JONSWAP spectrum versus Airy wave cases.

## 6.7 Limits

The relations that are found based on the figures such as Figure 6.7 can be compared to limits to the mechanical capacities of the cable. By doing this, an assessment can be made into the maximum allowable value of the motion parameters considered. As the cables vary quite significantly between manufacturers the limits also vary. Moreover, progressing insight in engineering shifts the limits over time. To capture these effects the limits are determined as high, middle and low scenarios, as displayed in Table 6.1. These numbers will be subject to the same normalization as the data points, as described in 6.5.

While there is limited public information about the mechanical limits of the cables considered, the tension, compression and curvature limits are primarily based on cables previously installed by Boskalis Subsea Cables. The tension limit for inter-array cables concentrates around the two values given in Table 6.1, with the majority of cables very close to the higher limit. The compression limit was for a long time determined to be zero, as a knowledge gap existed in the area of compression behavior. Currently, it is common practice to specify the cable compression limit at

10% of the tension capacity, following the work of Reda et al., 2016. The curvature limits are chosen to represent a range of the more restrictive limits from previously installed cables, with comparable cable diameters.

**Table 6.1.:** High, middle and low limits for the mechanical cable failure parameters.

Failure criterion	Low limit	Mid limit	High limit
Tension	50 [kN]	-	110 [kN]
Compression	0 [kN]	5 [kN]	10 [kN]
Minimum bending radius (Maximum curvature)	3.8 [m] (0.263 [1/m])	3.2 [m] (0.313 [1/m])	2.6 [m] (0.385 [1/m])

## 6.8 Parameter variation

The simulations described in this chapter are performed for a cable with specific properties, in a second end pull-in operation at a single location. This allows for the generation of detailed results for that case. In order to generalize the results, a parameter variation is carried out on the bottom tension, cable diameter, pendulum length, water depth and cable weight, as summarized in Table 6.2. This is done only for snapshot 2 and with the input cases from Section 6.3.

**Table 6.2.:** Parameter variations.

Parameter		Main analysis	Parameter variation
Bottom tension	[kN]	2.5	7.5
Cable diameter	[mm]	124	150
Pendulum length	[m]	varied per snapshot	Main + 5 m
Water depth	[m]	25	35
Cable weight	[kg/m]	25	34

# OrcaFlex modeling

“All models are wrong, but some are useful.

— **George Box**  
Statistician

As mentioned in section 6.1 the system configuration and environmental properties are implemented in an Orcaflex model such as in Figure 7.1. This chapter will describe what elements are used to model the configuration, what environmental effects are taken into account, which interaction effects are considered and how the model parameters and boundary conditions are determined and implemented.

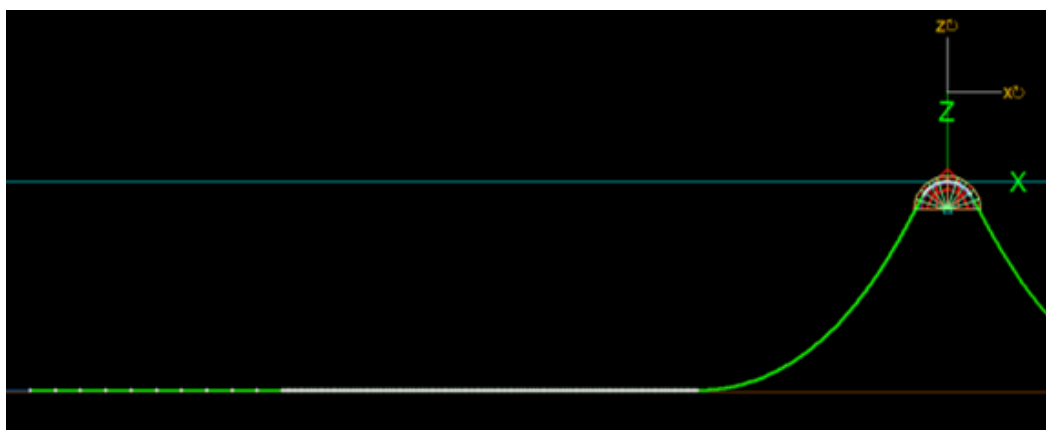


**Figure 7.1.:** The Orcaflex model for snapshot 2.

## 7.1 Model elements

The vessel is implemented in a separate Orcaflex model as a rigid body to which RAOs are assigned. All the properties are concentrated in the vessel center of gravity and are determined from a diffraction model. The model properties are given in Table 7.1 and Figure 7.2. A point of interest is added at the coordinates of the suspension point to track the motion of the point. This is used as input for the response of the cable-quadrant system.

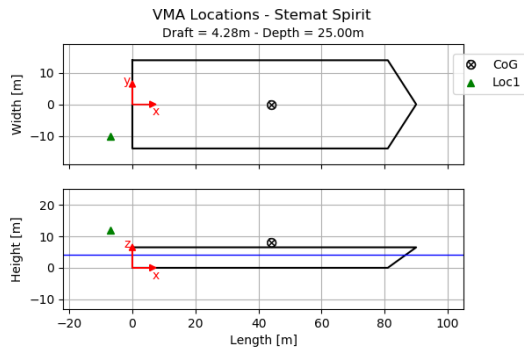


Figure 7.2.: Location of the suspension point.

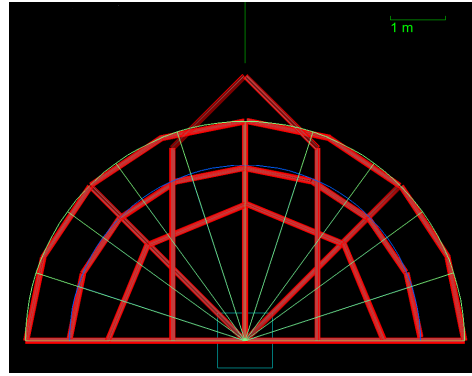


Figure 7.3.: Geometric model of the quadrant.

The crane wire is modeled in OrcaFlex as a link. A link is a simple connection with only the properties: initial positions of the ends, unstretched length and stiffness. This means that no hydrodynamic effects are taken into account on the crane wire. The top end is connected to the suspension point at a height of 12 [m], the stiffness is set at  $10^4$  [kN/m]. The unstretched length is 4.3 [m], 9 [m] and 27.7 [m] for snapshots 1, 2 and 3 respectively.

The quadrant is built up from tubular structural elements for the frame as displayed in Figure 7.3. These members are identical except for length. Each elements is modeled as a Morison element of which the parameters are displayed in Table 7.2. In modeling the quadrant with respect to the cable, this structural frame alone is not sufficient as it will not support the cable during simulation. In order to provide interaction with the cable, shapes are attached to the frame that contain defined geometries, normal stiffness and shear stiffness. Shapes are separate elements in Orcaflex. They do not interact with any element other than the cable. A shape is used to define the roller track geometry of the minimum radius of the quadrant as well as for the side support frames.

Table 7.1.: Vessel model properties.

Vessel property		Value	Unit
Mass	m	9214	[te]
Geometry	L*B	90x30	[m]
Draft	T	4.28	[m]
CoG	x	43.9	[m]
	y	0	[m]
	z	7.82	[m]
Suspension point	x	-7	[m]
	y	-10	[m]
	z	12	[m]
Moment of inertia	roll (x)	5.45E8	[kg/m <sup>2</sup> ]
	pitch (y)	3.47E9	[kg/m <sup>2</sup> ]
	yaw (z)	3.50E9	[kg/m <sup>2</sup> ]

Table 7.2.: Quadrant properties.

Quadrant members		Value	Unit
Diameter	D <sub>O</sub>	0.1	
	D <sub>I</sub>	0.066	[m]
Density	ρ	8000	[kg/m <sup>3</sup> ]
Drag	C <sub>d</sub>	1.5	[-]
Added mass	C <sub>a</sub>	1	[-]
Slamming		1.57	
<b>Quadrant shapes</b>			
Normal stiffness	k <sub>n</sub>	5E4	[kN/m <sup>3</sup> ]
Shear stiffness	k <sub>t</sub>	100	[kN/m <sup>3</sup> ]

The cable is the component of interest. It affects the system response the most and the cable integrity is what needs to be assured. The cable is therefore modeled to high precision and accuracy. It is implemented as a 3D line with mass, axial stiffness, bending stiffness, and torsional stiffness. Inertia, drag and friction are also incorporated, as elaborated on in section 7.2. The cable properties are implemented as presented in Table 3.1, Table 7.4 and Figure 3.8. While the necessary parameters were not all available for any one existing cable, a fictitious representative cable was modeled with all parameters set to a typical value for inter array cables.

The system configuration is determined to a large degree by the water depth. Off-shore wind farms are typically constructed at water depths between 10-40 meters. Therefore a representative water depth was selected of  $d = 25$  [m]. The seabed is modeled as a flat surface with a normal stiffness and a shear stiffness of  $100$  [ $kN/m/m^2$ ]. The system is excited through the motion of the suspension point generated by the vessel response to the sea states described in Section 6.3. The time record of the sea state is also applied to the cable and quadrant directly. No wind and current are considered as they represent relatively low magnitude or slowly varying loading conditions.

In order to recreate the catenary shape, the boundary conditions for the static calculations were implemented in the form of winches with constant pull force of  $T_0 = 2.5$  [ $kN$ ], with cable friction set to zero. After converging to the static solution the cable ends are fixed, cable-soil friction and cable-quadrant friction is applied and the winches are removed. The static equilibrium position of the system is now achieved.

## 7.2 Interactions

In the dynamic analysis the hydrodynamic reaction to cable motion is of key importance. For slender structures in oscillating flow the reaction force is given by the Morison equation incorporating the velocity related drag component and the acceleration related inertia components:

$$F = F_I + F_D = (m a_f + m_a a_r) + \frac{1}{2} C_D D u_r^2 \quad (7.1)$$

This equation is divided into the inertia of the cable mass itself, the added inertia (added mass) of the surrounding water and the drag component. The drag contribution is given below in equation 7.2 while the inertia effect is given in equation 7.3.

$$F_D = \frac{1}{2} C_D D u_r^2 \quad (7.2)$$

The drag force is related to the relative velocity between the cable and the surrounding fluid through the drag coefficient. This drag coefficient depends strongly on the flow conditions around the body and is determined to be  $C_D = 1.2$  for most

conditions applicable for this thesis. A more detailed consideration is presented in appendix B.

$$F_I = F_{FK} + F_{am} = C_f m a_f + C_a m a_r \quad (7.3)$$

The inertia contribution is divided into the Froude-Krylov component and the added mass component. The Froude-Krylov component represents the force that would be exerted on the body by the oscillating fluid under the condition that the body does not disturb the flow. It is determined by the flow acceleration relative to earth. The added mass component represents the inertia of the wave field disturbance generated by the body. It is determined by the flow acceleration relative to the body.

Where it holds for equations 7.1, 7.2 and 7.3 that:

$F_D$	= Drag force [N]	$F_I$	= Inertia force [N]
$C_D$	= Drag coefficient [–]	$C_f$	= Froude-Krylov coefficient [–]
$D$	= Diameter [m]	$C_a$	= Added mass coefficient [–]
$u_r$	= Relative velocity [m/s]	$a$	= Acceleration [m/s <sup>2</sup> ]
$m$	= Mass [kg]	$a_f$	= Acceleration relative to fixed reference [m/s <sup>2</sup> ]
$m_a$	= Added mass [kg]		

Practically, calculating the magnitude of normal and tangential contributions to the inertia and drag effects is achieved by decomposing the motions. The accelerations and velocities are transformed into motion parameters in the local coordinate system of the element it acts upon. From this the normal and tangential contributions are determined in order to incorporate the different coefficients, after which they are transformed back into forces in the global main axes.

Both the quadrant shapes supporting the cable and the seabed are modeled as linear elastic solids. A normal stiffness is specified for each, as well as a shear stiffness. The quadrant is a heavy duty steel structure which behaves almost as a rigid body. Therefore it has high normal stiffness. The seabed stiffness is more difficult to determine. The boundary between water and soil is not always well defined and the cable may penetrate the seabed to some degree. When lifting the cable from the seabed suction may in reality add damping. This is not modeled in Orcaflex as the calculation method restricts this (as mentioned in section 5.4). The stiffness is considerably lower than the quadrant stiffness. The shear stiffness in conjunction with the friction coefficients specified between surfaces defines the resistance to sliding of the cable. The coefficients are given in Table 7.4.

## 7.3 Verification

To verify the calculation process used by Orcaflex the results are compared to a model implemented in python based on information given in Chapter 4.2 and taken from literature. This model incorporates an iterative algorithm to find the configuration

of the cable in response to a motion applied at the top node of the catenary. Both results are compared to the analytic catenary equation to see if the configurations match in the static situation.

**Statics** The statics of the catenary are calculated in three ways for the same situation. The node positions and segment tension are determined by the catenary equation as mentioned in equation 4.3, by means of a Newton Raphson iteration and by making use of an Orcaflex model. For the simple case of a catenary the results closely resemble each other.

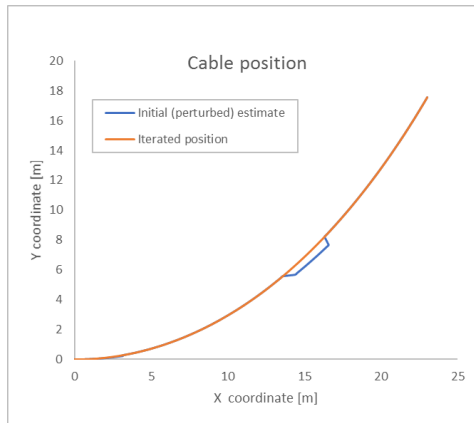


**Figure 7.4.:** Catenary position after Newton Raphson iteration with perturbed initial estimate based on analytic catenary.

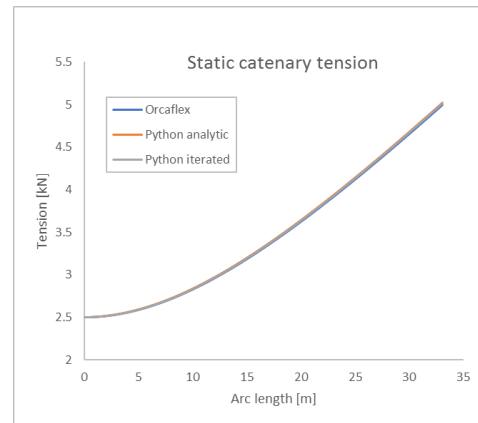


**Figure 7.5.:** Catenary tension as determined by the catenary equation, NR-iteration and orcaflex model.

The Newton Raphson iterator takes an initial estimate of the cable position and iterates the positions and the tensions until convergence is reached. The initial estimate of the NR iterator is the analytic catenary result with a perturbation included. Provided that this initial estimate is relatively close to the real situation, the iterator will converge to the solution. The initial estimation of the cable and the converged cable position are plotted in Figure 7.4. The tension in this situation is plotted in Figure 7.5 along with the tension obtained by the catenary equation and the Orcaflex model. The results show very good correspondence.

**Sensitivity & convergence** As convenient and extensive as Orcaflex is to analyze a wide range of situations, if the input is erroneous the output will be too. To verify that the models that are applied are correct and suitable to analyze the situations of interest, a sensitivity analysis is performed. The sensitivity of the models to pendulum length variations, a submerged or emerged quadrant and variations in hydrodynamic coefficients of the cable and the structural elements of the quadrant are investigated in model 1. Issues regarding solution method of the equations of motion, the time step size, segmentation length, seabed modeling and damping

implementation are covered by model 2. The modeling and configuration of this sensitivity study is described and illustrated in detail in Appendix D.

From a convergence study the parameters in Table 7.3 were determined to have shown convergence at the value listed. The parameters in Table 7.4 show significant influence on the results but did not converge to a single solution for a range of values, and are therefore determined from literature or assumed at the value presented.

**Table 7.3.:** System parameters obtained from convergence study.

Parameter	value	unit
Time solve method	implicit	
Time step	constant	
Time step size	0.01	[s]
Segment length	0.3	[m]
Rayleigh damping	0	[%]

**Table 7.4.:** Implemented drag, inertia and seabed friction coefficients. \*Value depends on  $Re$  (see Figure B.1).

		Normal	Axial
Drag	$C_d$	1.2*	0.01
Froude-Krylov	$C_m$	1	1
Added mass	$C_a$	0.9	0
Seabed friction	$C_{sb}$	0.4	0.2
Quadrant friction	$C_q$	0.1	0.1

In addition, the following effects are observed:

1. The pendulum length has little to no influence on bend radius near the extremes. It does however impact tension near the quadrant and compression throughout the line.
2. Submerging the quadrant increases both maximum compression near the touchdown point (TDP) as well as maximum tension near the quadrant.
3. Varying the hydrodynamic coefficients of the structural elements of the quadrant influence the cable response. However, it is noted that these elements are in the hydrodynamic area of influence of each other. Interaction effects will therefore play such a significant role that the only way to accurately determine the coefficients is to do a physical model test and determine them for the quadrant as a whole. However, this is outside the scope of this thesis.

**Parameter variations** To generalize the results obtained by the model described in this chapter, a parameter variation is performed. This comprises the modification of the model of snapshot 2 in certain parameters that have a wide range of realistically occurring values. In addition, some parameters can consciously be altered to tune system to show more favorable behavior. The parameters that are checked are the water depth, the cable diameter, the submerged cable weight per unit length, the pendulum length and the bottom tension.

# Results

## 8.1 Normal cable laying

In the model described in Chapters 6 and 7 the quadrant supports the cable hanging off both sides. This system is suspended by a crane wire to the crane tip on the vessel, allowing the quadrant to perform pendulum motions. Eliminating some elements of this model creates a model similar to that used to assess compressive cable behavior in the continuous laying process as carried out in precursory research (Loos, 2017). By imposing motions on the quadrant directly and eliminating the crane wire and one of the catenaries the quadrant reduces to a model similar to the chute on the stern of the CLV. A comparison between the results of this model and the precursory research is displayed in Figure 8.1, of which the green data points in the right figure display the configuration that most closely resembles the configuration used in this thesis. Most notably, the departure angle is nearly identical. The figure shows the same qualitative behavior between the two studies, granting a degree of verification to the model used here. This is true even while most other configuration and cable parameters such as water depth, cable weight and cable diameter are significantly different. In addition to this, the imposed motions applied here are not only axial motions, but also horizontal and vertical motions from which the component in axial direction is plotted versus the tension loss. In the previous work only motions in, and close to, the axial direction were applied. This explains the larger spread in the left figure.

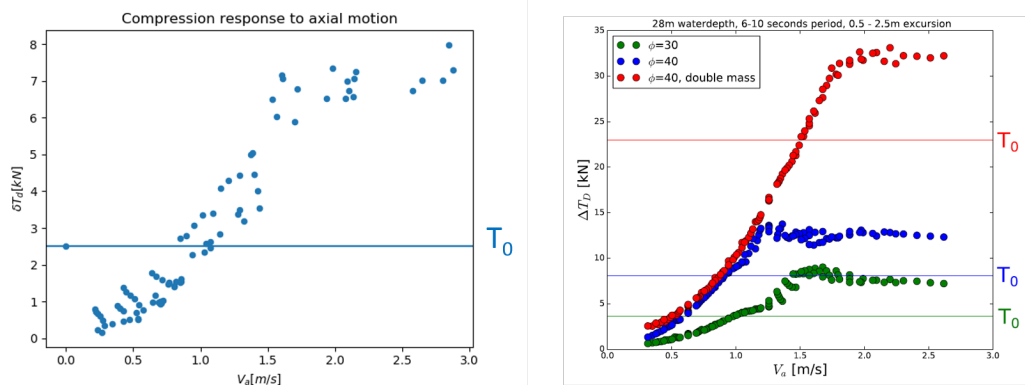


**Figure 8.1.:** Results from the current investigation (left) and that of previous work (right, taken from (Loos, 2017)).

## 8.2 Preliminary observations

As mentioned in Section 6.3 and Figure 6.7 the sea states are applied to the vessel and the cable-quadrant system in both JONSWAP and Airy wave trains with the same respective wave height and period parameters. While the results for each analysis case differ for the JONSWAP and Airy wave simulations, no underlying bias is observed. When spreading in the results of Airy waves are large for any two compared parameters, the same holds for JONSWAP and vice versa. Conversely, when the results of either Airy or JONSWAP waves closely define a correlation between input and output, the other wave type shows the same behavior, even converging to the same relation. This is displayed in Figure 8.2.

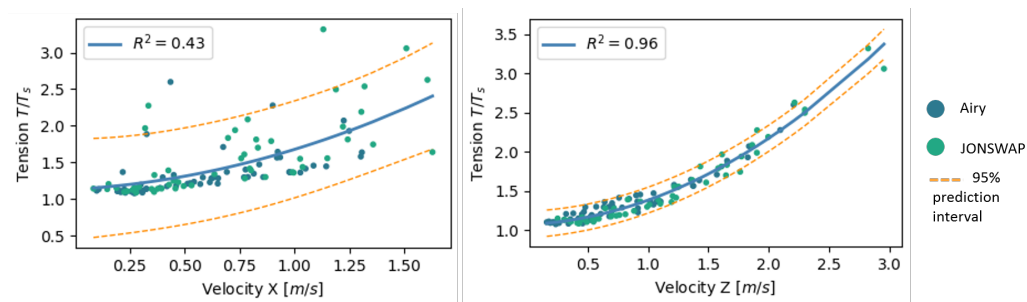


**Figure 8.2.:** Comparison between JONSWAP and Airy waves for a case with low correlation between input and output (left) and a case with close correlation (right). Both panels display results for snapshot 2: splash zone.

In Figure 8.2 the dependent parameter (tension for this case) is plotted against a positive input parameter (sway motion for the left panel, heave for the right panel). However, for motions in the negative directions, the cable response is different. For tension the closest correlations are found in the positive motion directions, but for both compression and curvature the negative motions produce clearer relations, as indicated by the check marks in Figure 8.3.

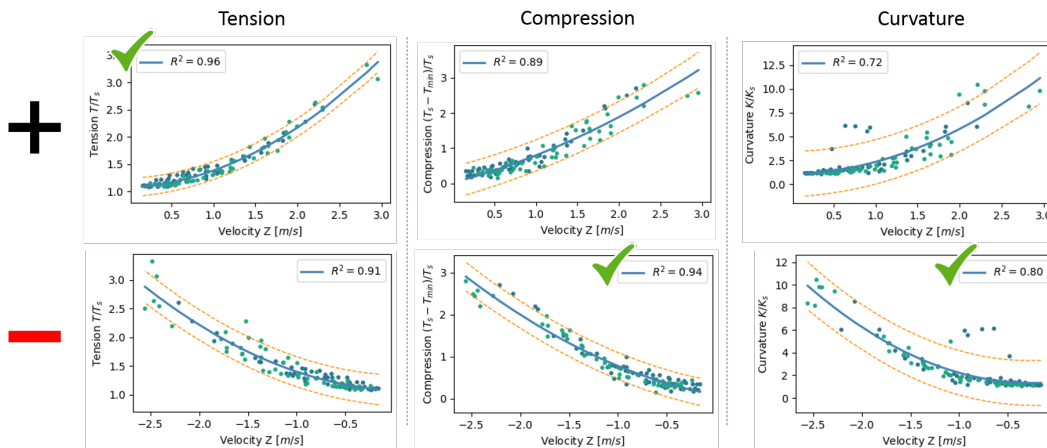


**Figure 8.3.:** Comparison between curve fits for output parameter correlation to positive and negative input.

In Figure 8.3 the tension, compression and curvature response is shown only in relation to heave motion. Figure 8.4 displays why this motion is emphasized. It shows that heave motion is the best indicator of the tension response, as seen in the middle right panel. Although not displayed, for compression and curvature this is true as well and the observation holds up across all three snapshots.

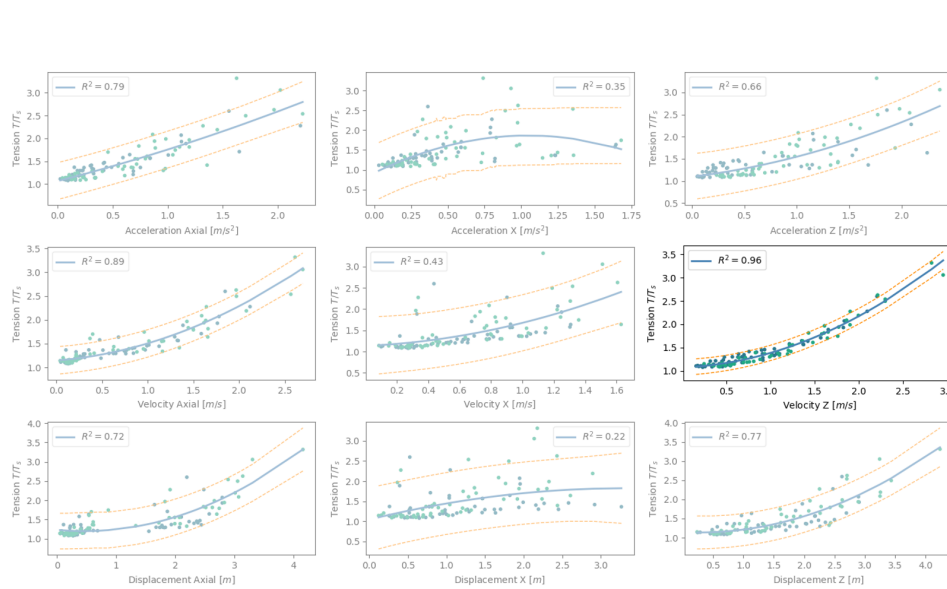


**Figure 8.4.:** Tension related to different input motions for snapshot 2. The correlation with heave is the closest.

## 8.3 Relations

In Figures figures 8.5 and 8.6 the results are displayed as reported in Section 6.6. Each panel in the figures displays the best fit curve for the particular failure parameter for that snapshot in relation to the input. For each of the panels, 8 figures are not shown, since the relation between motion parameter and reaction parameter is less correlated. From figures 8.5 and 8.6 it can be determined that tension in all snapshots is closely correlated to heave velocity. A distinction is also apparent between positive motion (up) and negative motion (down), where maximum tension is more closely related to positive motion in snapshots 1 and 2. For snapshot 3 the opposite holds. Compression in the line is also correlated to heave velocity for all snapshots. However, for compression it is the negative heave motion (down) that is most determinative. The correlations are marginally lower for compression across all three snapshots when compared to tension. Curvature shows the closest relation to downward heave velocity for snapshots 1 and 2. The correlations are somewhat lower than for tension and compression. Curvature in snapshot 3 is related most to heave displacement, where up- or downward motion shows no difference in correlation.

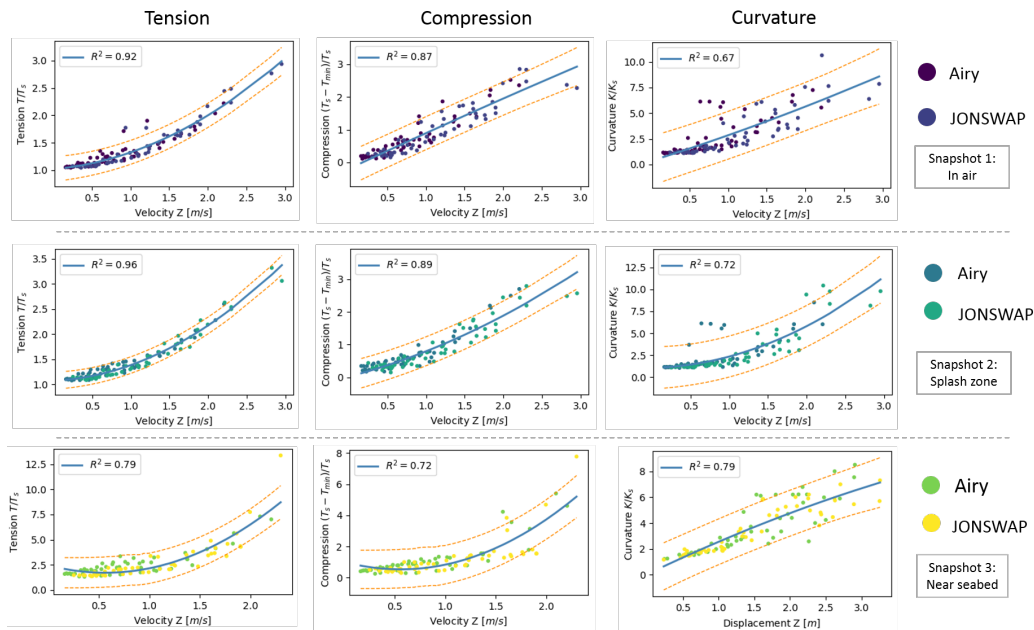


**Figure 8.5.:** Mechanical cable response as a function of suspension point motion in **positive** motion direction for the most correlated cases based on the  $R^2$  score.

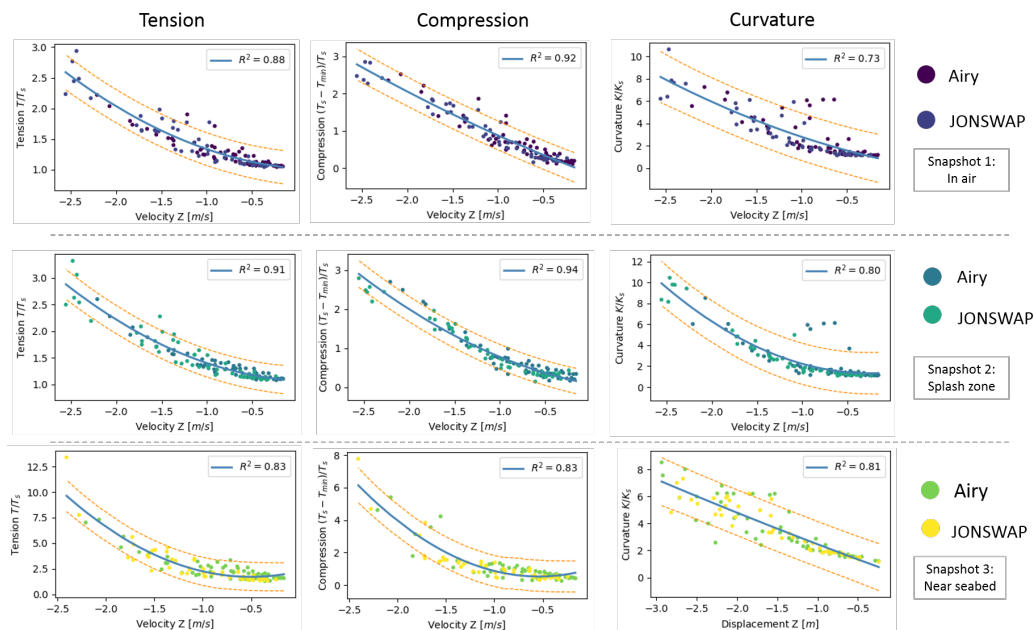


**Figure 8.6.:** Mechanical cable response as a function of suspension point motion in **negative** motion direction for the most correlated cases based on the  $R^2$  score.

In some of the curves describing the closest relations for input and output parameters small clusters of outliers can be observed. This is the case for tension and compression with the quadrant in air. These cases all correspond to load cases with large sway motions of the suspension point with a periodicity of 5 [s]. This corresponds roughly with the pendulum natural frequency of the quadrant hanging from the suspension wire, which should be avoided. Another set of outliers is found for curvature in all three snapshots, although they are less pronounced when the

quadrant is near the seabed. These also correspond with large sway motions of the suspension point, now with periods of 15 [s] and up. These low frequency outliers influence the exceedance of limits.

## 8.4 Limits

Applying the limits in figures gives the view presented in Figure 8.7, where the horizontal lines represent the normalized limits for the given mechanical cable property. Note that these limits change values depending on the static situation of the snapshot. From the figure it follows that the maximum cable tension limit is of no concern for any situation investigated. Compression remains well below the most lenient limit for snapshots 1 and 2. While the middle limit is not exceeded by any actual simulation in snapshots 1 and 2, the prediction interval does exceed it. The strictest limit is exceeded in every snapshot. For snapshot 3, each limit is exceeded by multiple simulations. The curvature limits are exceeded for every snapshot. The curvature is affected by the outliers when it comes to exceedance of the failure envelope. This effect is displayed in Figures 8.7 and 8.8. The difference in the two figures is the effect of low frequency outliers.

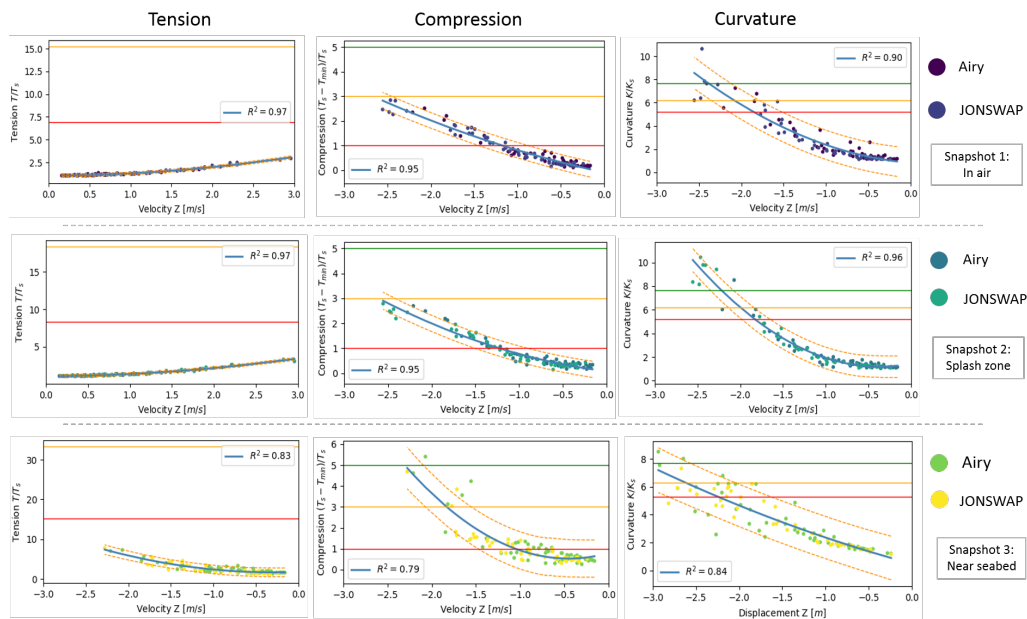


**Figure 8.7.:** Mechanical cable response as a function of suspension point motion including the normalized limits. Only the most correlated cases are displayed. The outliers due to resonance described in Section 8.3 as well as the low frequency outliers have been removed.

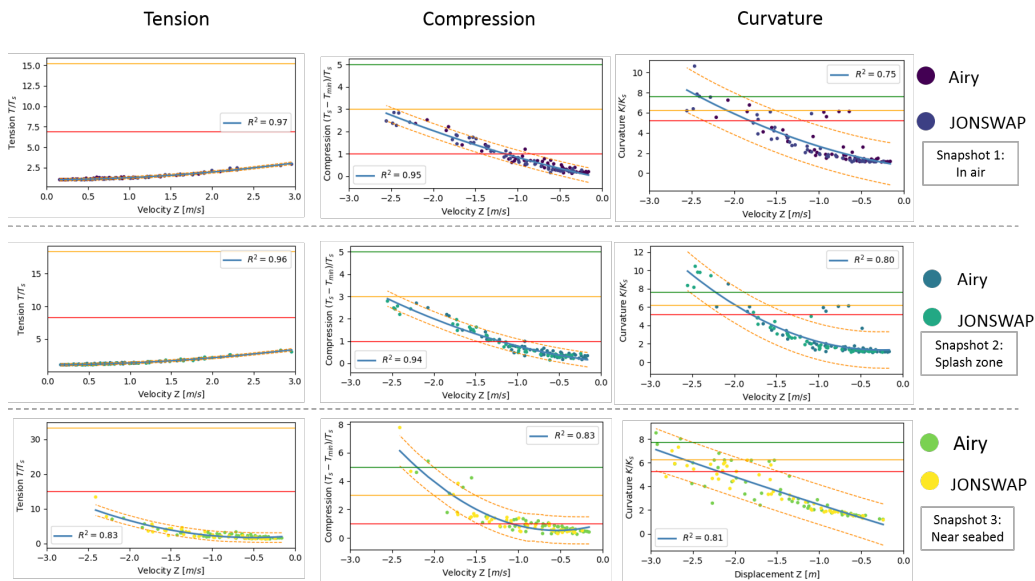


**Figure 8.8.:** Mechanical cable response as a function of suspension point motion including the normalized limits. Only the most correlated cases are displayed. The outliers due to resonance described in Section 8.3 have been removed.

## 8.5 Wave loading

The presence or absence of waves directly loading the cable and quadrant has an effect on the relations. For snapshots 1 and 2 the only significant change is observed in the curvature graph, where higher curvature extremes and a slightly better correlation is observed when wave loading is disregarded. These effects are displayed in figures 8.9 and 8.10. For snapshot 3 the compression dependence on downward heave velocity decreases somewhat when direct wave loads are not considered. The dependence on downward heave displacement of the curvature increases quite significantly. The differences are visualized in figures Figure 8.11 and Figure 8.12.

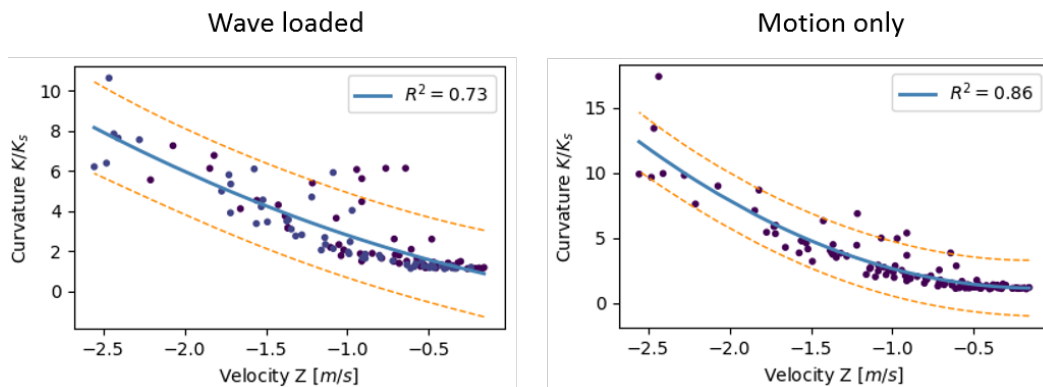


**Figure 8.9.:** Direct wave loading effect for snapshot 1 on the relation between downward heave velocity and curvature.

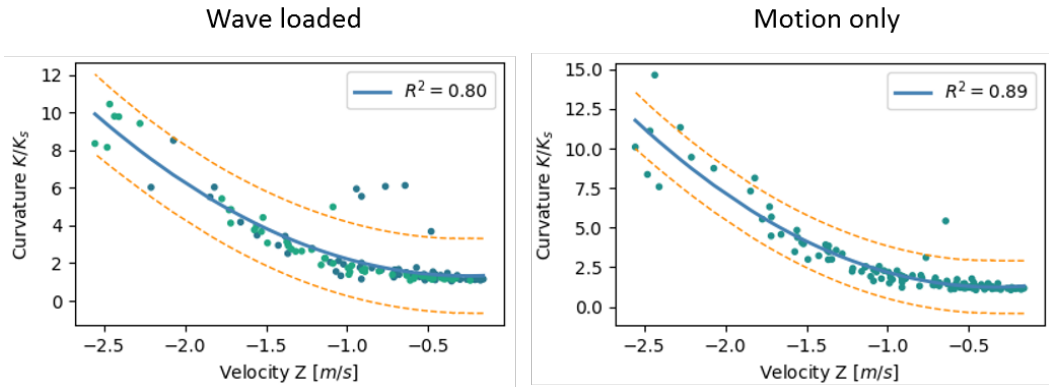


**Figure 8.10.:** Direct wave loading effect for snapshot 2 on the relation between downward heave velocity and curvature.

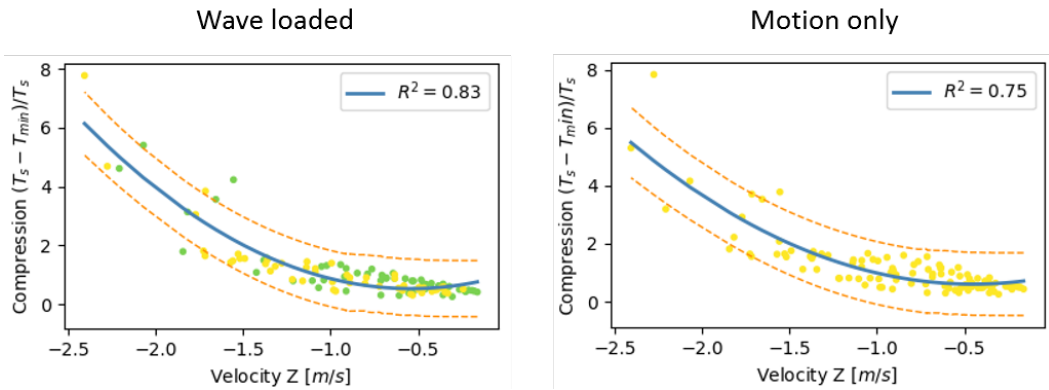


**Figure 8.11.:** Direct wave loading effect for snapshot 3 on the relation between downward heave velocity and compression.

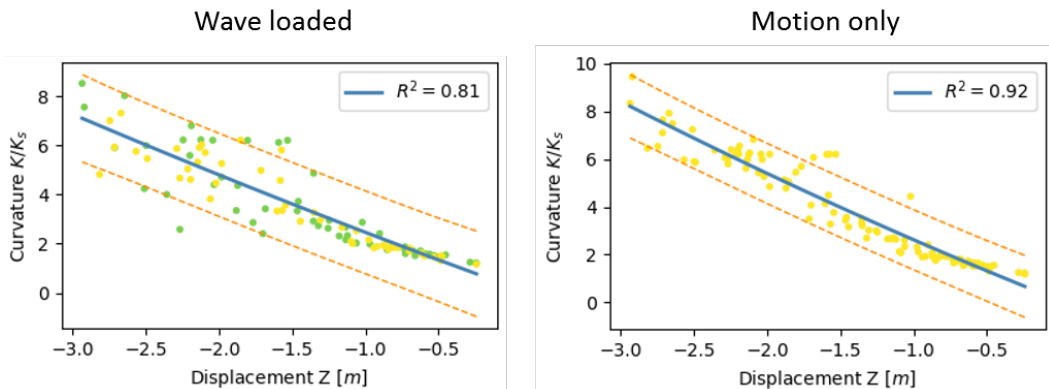


**Figure 8.12.:** Direct wave loading effect for snapshot 2 on the relation between downward heave displacement and curvature.

## 8.6 Parameter variations

By introducing parameter variations it is investigated if the correlations hold for different configurations. By doing this the static situation of the configuration is changed which has implications for the normalization applied to the system. Not only may the system behavior be impacted, the limits will also change in the normalized visualizations.

Behavior of the system changes slightly for tension in response to varying system parameters. However, no case comes close to even the strictest tension limit. Compression behavior of the cable is notably changed by increasing the bottom tension on the system. The 5% compression limit is expected to be exceeded at a much lower downward velocity compared to the base case, as is displayed in Figure 8.13.

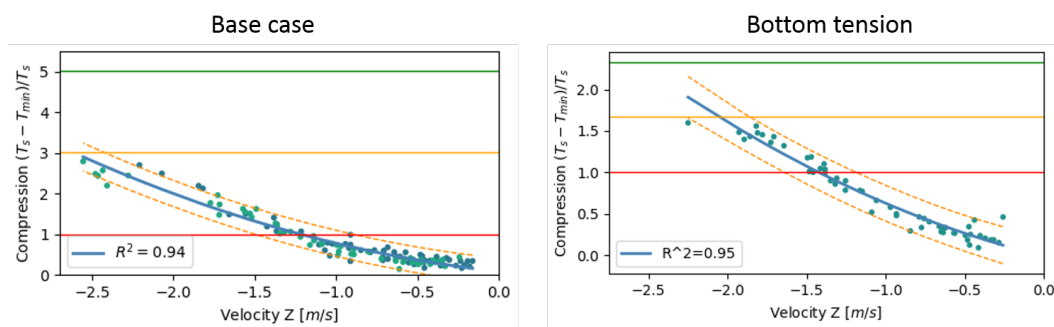


**Figure 8.13.:** Parameter variation effect on compression.

The curvature behavior is the most sensitive to parameter variations. Various effects can be observed in Figure 8.14. The relation of the curvature to downward heave is no longer present for the case with increased bottom tension. Instead, the negative horizontal motion becomes most determinative. While the other parameter variations do not produce such differences in the relations, an effect is observed on the outlier data points. The outliers reduce or disappear in the diameter, weight and water depth variations. Overall, the velocities at which the prediction interval intersects the limit lines changes only slightly, with the diameter increase showing the most unfavorable effect.

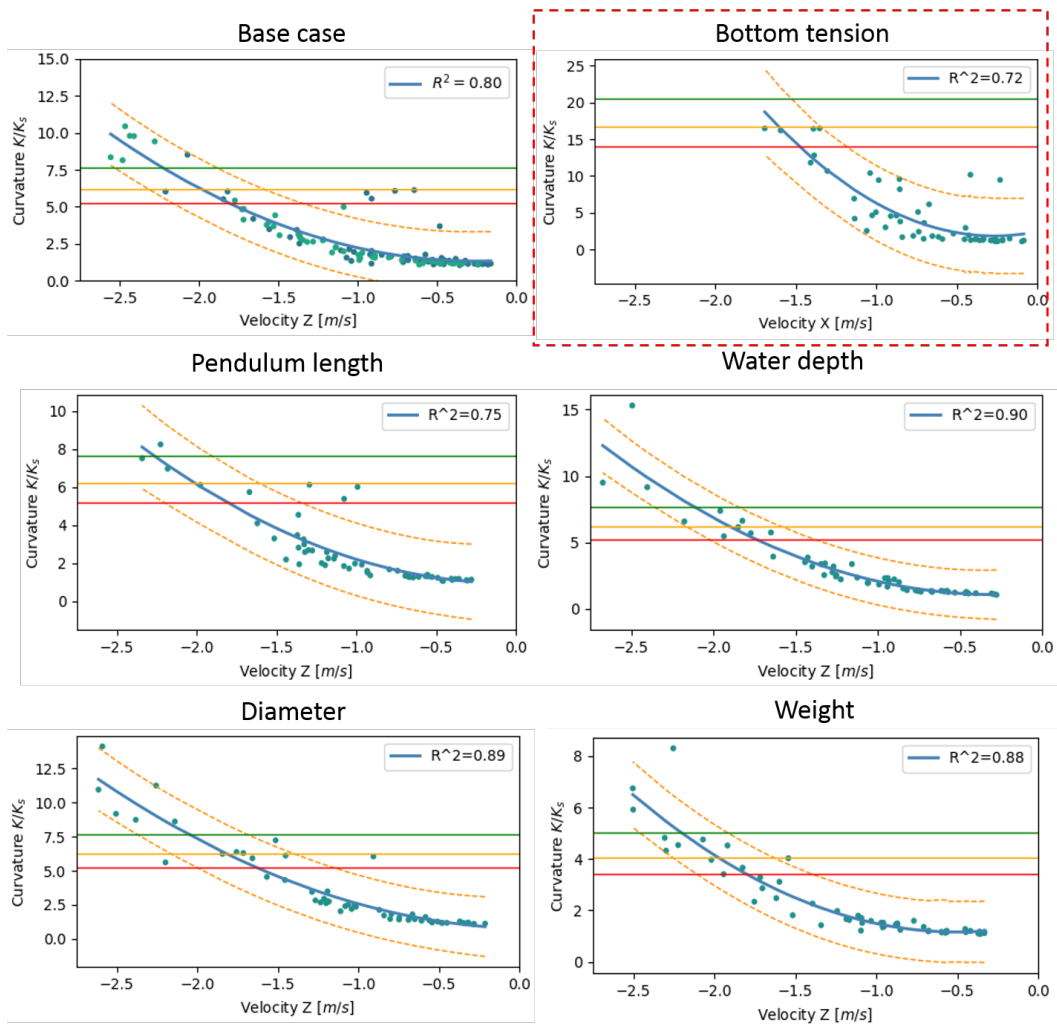


**Figure 8.14.:** Parameter variation effect on curvature. Only the most correlated relations are shown.



# Conclusions & recommendations

## 9.1 Discussion

**Validity** The results in this thesis were obtained using Orcaflex. This piece of dynamic analysis software is an industry standard in the field of pipeline, riser, umbilical and cable installation. It is verified and validated against other software and real world data for a range of applications, of which cable analysis is an important case. For the analysis performed, a set of time domain calculations was carried out on a segmented length of cable. Setting the time step of the calculation and the segment length to of the cable to a correct value determines to a large extent if accurate results are obtained. A convergence study was carried out to find the largest values for which the end results no longer change with respect to the smaller step sizes and these were implemented. This ensures that the computational load remained manageable while all the effects of interest were correctly represented within the capabilities of the program.

Most analyses are performed on a model with a specific set of properties and conditions representative of actual situations. To expand the amount of situations to which the conclusions are applicable a set of parameter variations is carried out. In this parametric variation the effects of increased water depth, bottom tension, cable diameter, cable weight and pendulum length was investigated. For these cases the same qualitative relations hold between suspension point motion and cable response.

**Interpretation** The first thing that is obvious when reviewing the results is that heave motion is the dominant factor for all cases. This dominant impact on the response is divided into upward heave velocity when it comes to the maximum tension response, downward heave displacement for curvature in snapshot 3 and downward heave velocity for all other cases. The reason for this can be derived from the forces acting on the quadrant in the static situation. The quadrant is loaded by the self weight and the weight of the cable, directed straight down. This force is compensated by the crane wire, the force of which is directed straight up. Any horizontal component in upward motions of the suspension point can not be transferred to the quadrant until the suspension point has moved considerably. When this happens, the quadrant will perform a pendulum motion that is damped by the cable catenaries. Any motion directed straight up will be transferred to the quadrant by a large elastic force in the crane wire, which in turn generates an upward motion of the quadrant and therefore a response in the cable. For downward motion a similar effect occurs. In this case the crane wire force reduces, making the quadrant drop.

Again, any horizontal components of the suspension point motion is not initially transferred to the quadrant as gravity will force it straight down. After the initial downward motion of the quadrant it will again perform a pendulum motion. Any motion of the suspension point that is directly aligned with the forces acting on the quadrant in the static situation (gravity and the elastic crane wire) will therefore generate the greatest response in the cable.

**Limitations** Although the investigations carried out in this thesis model the quadrant assisted pull-in operation to a good degree, some issues have arisen that limit the applicability of the obtained results.

When analyzing the cable response to a given excitation, accurately modeling the cable-quadrant system is important. Although most elements have been taken into account, some effects have been disregarded to keep the modeling process manageable. In a real 2<sup>nd</sup> end pull-in the cable would be fitted with a CPS. This protective sleeve around the cable connecting the cable to the foundation entry point is designed to prevent overbending of the cable and protect it from foreign objects. This CPS could influence the response of the cable to the excitation as the diameter, weight and bending stiffness are all considerably different from the cable and a significant length of cable may be fitted with it. The CPS is not considered in the scope of this thesis, as are any interaction effects with the wind turbine foundation or any other rigid bodies in the vicinity.

From the generated results it follows that while the tension shows a close dependence on heave velocity, the tension range that is obtained remains below the limit by a large margin. This indicates that the used configuration is not critical in tension loading. For deeper waters and higher cable weights, the generated tensions in the cable will increase. While the dependence on heave velocity is expected to remain present based on the reasoning described above, the behavior of the system near the cable tension limit can not conclusively be determined from the results of the current investigation.

## 9.2 Conclusions

In this thesis an investigation was carried out into the relations between vessel motions and mechanical cable integrity limits for a quadrant assisted cable pull-in operation. Initially an investigation was performed into the current method of analysis. Additionally, a literature review was carried out to determine what loads may be exerted on the cable in this situation, as well as what failure modes may be expected to occur. On this basis, a set of simulations was performed in order to find the relations between the vessel motion and the cable response with respect to the cable response limits. For convenience the research questions from Section 2.2 are repeated here:

## What are the relations between vessel motions and cable integrity limits for the quadrant assisted pull-in operation?

1. What physical properties and processes play a significant role in cable loading during quadrant assisted pull-in?
2. Which cable failure modes may be activated by the operation and what limits on cable response do they impose?
3. What are the relations between vessel motion and cable response?
4. What are the governing limiting motion conditions of the vessel on cable integrity?

**Cable loading and failure modes** Hydrodynamic response of the cable is of key influence. It is defined by the diameter of the cable and the motion conditions. Near the failure regions of the cable, the hydrodynamics are drag dominated. A correct implementation of drag coefficient is therefore essential.

Excitation of the cable-quadrant system originates from the sea state, both through vessel excitation and direct wave loading on cable and quadrant. The effect of vessel motion is most important. However, direct loading does affect the cable response to a significant degree in certain cases and must be accounted for to avoid underestimation of the cable response.

**Limits** The modes in which cable integrity may be compromised are due to tension, compression, curvature, squeeze load and side wall pressure. However, squeeze load and side wall pressure are associated most with loading conditions outside of the second end pull-in operation and are therefore not considered here.

The tension limits for a range of cables concentrate around the values of 50 [ $kN$ ] and 110 [ $kN$ ]. For compression, a limit of zero has long been applied. Recent new research has allowed for approximately 10% of the tension limit to be present as compression, respectively 5 [ $kN$ ] and 10 [ $kN$ ]. Bending radius limits vary heavily, ranging from a strict 3.8 [ $m$ ] to less problematic values below 3 [ $m$ ].

**Relations** From the results it is evident that the maximum tension occurring in the cable is related very closely to the heave velocity of the suspension point, regardless of the quadrant being in air, in the splash zone or near the seabed. In particular the upward heave velocity shows close correlation with tension.

Compression in the cable also shows a relation to heave velocity in all three configurations. However, for compression the downward heave velocity is governing. The curvature behavior shows slightly different dependencies and is generally slightly less correlated to the governing motion than tension and compression. While the quadrant is in air or in the splash zone the downward heave velocity is governing for cable curvature. However, when the quadrant is near the seabed the downward heave displacement has the largest influence on curvature.

The application of waves to the vessel in the form of regular Airy waves and irregular JONSWAP spectra result in much the same relations. While the spreading differs a

lot between the two wave types for most cases, in the closest correlated cases the difference is negligible.

The effect of waves directly loading the quadrant and cable in addition to the top motion excitation is small but not negligible. Although the cable response differs with direct loading applied, it is not possible to make a general statement as to whether it increases or decreases the vessel motion limit.

Varying the configuration parameters impacts the correlations to varying degree. The tension limits are well out of range for any parameter variation. Compression behavior is sensitive to the bottom tension, where the higher tension decreases the maximum allowed vessel motions. Curvature behavior is impacted most by parameter variation. It is most notably affected by an increase in bottom tension, where the correlation becomes closest for the negative horizontal motion. The other parameter variations show less impact, although an increased cable diameter brings down the allowed vessel motions to some degree.

In the results some closely clustered outliers were observed. Some of these outliers were caused by sway motion of the suspension point in the pendulum natural frequency of the quadrant hanging in air. This needs to be avoided for the relations to hold. Another cluster of outliers appeared in the low frequency range of curvature in all three snapshots. The reason for these outliers has not been determined and requires further investigation.

**Vessel motion limits** In the performed analyses the cable tension limits were never exceeded, regardless of the quadrant position. The zero limit on compression is problematic for values of the downward heave velocity as low as 0.5 [m/s] with the quadrant in air or in the splash zone, and would make the situation with the quadrant near the seabed completely unworkable. In the 5% and 10% compression limits the situation with the quadrant near the seabed is most limiting, with downward heave velocity limits of 1.5 [m/s] and 2 [m/s] respectively. The limits from curvature exceedance range from 1.2 [m/s] to 1.9 [m/s] downward heave velocity and from 1.5 [m] to 2.5 [m] downward heave displacement.

Tuning the bottom tension has a profound effect on the normalized limits in both compression and curvature. Increasing the bottom tension increases the normalized curvature limit. In contrast, it reduces the normalized compression limit.

**Main conclusions** From all the previous considerations it can be concluded that relations between vessel motions and mechanical cable responses are present for quadrant assisted pull-in operations. The dominant motion direction of the suspension point from which a response can be determined is heave velocity: directed upward for tension response, directed downward for compression as well as for curvature with the quadrant in air and in the splash zone. For the quadrant near the seabed the downward heave displacement is most determinative. Comparing these criteria to the limit values of the corresponding response parameter gives a statement about the operability of the situation.

An interesting effect that can be observed is that increasing the bottom tension

reduces the risk of the curvature limit being exceeded, while at the same time it increases the risk of the compression limit being exceeded. It could be a valuable tool in tuning a system to remain within the allowed limits.

## 9.3 Implications

The conclusions of this research fulfill several of the objectives posed in Section 2.1, which are repeated here:

**Define 'vessel motion' based operation limits for quadrant assisted pull-in operations for which cable integrity is preserved.**

Finding these limits would make it possible to analyze the problem in a frequency domain assessment. In doing so it is aimed to achieve:

1. Generation of knowledge and insight in the physics involved in quadrant assisted cable pull-in operations leading to an improvement in engineering methodology.
2. A linearization of the problem leading to a reduction in engineering intensity.
3. A reduced need for time domain analyses leading to lower computational requirements for the analysis of the problem.
4. Identifying key areas for improvement of workability in the second end pull-in process.

**Implications and recommendations** With the results that are obtained from the investigation it is determined that there is a relation between vessel motion and cable response in the quadrant assisted pull-in. In other words, the cable response can be expressed in terms of vessel motion.

With this knowledge it is possible to augment and improve the current analysis method. The most notable implication is that the problem can be solved in the frequency domain, once the relation between vessel motion and cable response is known for the specific cable, configuration and parameters. The procedure to be followed would consist of the following essential steps:

1. Build an Orcaflex model incorporating the relevant properties.
2. Estimate the maximum occurring motions of the vessel based on the vessel motion analysis compared to operating limits other than those induced by cable failure.
3. Create a set of small time domain analyses with imposed suspension point motions up to and slightly above the maximum occurring motions.
4. Determine the relations and suspension point motion limits for the specific case.
5. Analyze the vessel in the frequency domain to determine if the suspension point motion exceeds the motion limit.

With the application of the polynomial regressions and the corresponding 95% prediction intervals, the problem of analyzing the second end pull-in operation has been linearized. This allows for the analysis of the problem in the frequency domain based on vessel motions. While this will reduce computational requirements, acquiring the linear relations requires a comparable amount of engineering work as the current analysis methodology. The objective of reducing the required engineering effort has therefore not yet been achieved within the scope of this thesis. Now that the cable limits are shown to correlate in a curvilinear way to the vessel motion, further research into a closed formula is encouraged.

As the simulations for various load cases converge to the same curvilinear relation for each pair of motion input and cable response parameters, the relation can be determined from a relatively small set of simulations. In addition, the same simulations can be used for other pairs of input and output. The difference between JONSWAP wave spectra and regular Airy waves on the response is very small. Therefore, each simulation only needs to be as short as 3 to 5 wave periods of the load case specified by the vessel motion analysis. Once the relations are found and have been used, they can be added to a database of curves as they retain useful information. With each project the database can be expanded and with enough relations in the database, interpolation between curves becomes possible. Unfortunately, each configuration still needs time domain simulations. The efficiency gain is therefore less than anticipated.

An important thing to notice is that in all investigated cases heave (displacement as well as velocity) was the dominant motion direction of the suspension point from which the cable response could be derived. This indicates that heave compensation on the vessel crane could be considered as a way to increase workability for the pull-in operation from a cable integrity point of view.

With the polynomial regression and prediction interval in place, the response of the cable is defined continuously for suspension point motion input. Discretization uncertainty is therefore no longer present in the results. This will open up some situations near the limit for the vessel to operate in.

**Further research** While the conclusions drawn here provide a new insight in the governing parameters defining cable loading during quadrant assisted pull in operations, further research is required to comprehend the problem more thoroughly. For instance, the motions of the vessel generated by the waves were in this research transmitted to suspension point in two directions only. This was done to narrow down the investigated parameters. An investigation into the behavior of the system with a suspension point free to move in all directions is required to get a grasp of all the factors at play.

Another simplification applied here, was the absence of interaction effects with a CPS or rigid structures in the vicinity of the cable. Incorporating this in the model could change the results significantly. The changes could originate from snatch loads occurring, non symmetrical weight distribution over the cable or wave interaction effects around the foundation.

While the results of this thesis are promising, a closed formula containing known

parameters that predict the cable response for a general case is not yet found. Expanding the set of simulations or performing a meta study on previously analyzed practical cases could generate more insight in how to predict the response without the need for any time domain simulation at all in the future and is therefore greatly encouraged.



# Bibliography

- Betts Berklite, Ronald (1972). „Adde mass of submerged objects of arbitrary shapes“. MA thesis. Naval Postgraduate School, Monterey California (cit. on p. 72).
- BPP Cables (2017). *High-Level Study on the Potential Impact of Rollers on Subsea Power Cables*. Tech. rep. (cit. on p. 22).
- BSCF (2018). *Boskalis specification sheet quadrant MBR 2.5m* (cit. on p. 12).
- Cha, Ju-Hwan, Myung-Il Roh, and Kyu-Yeul Lee (2010). „Dynamic response simulation of a heavy carco suspended by a floating crane based on multibody system dynamics.“ In: *Ocean Engineering* 37 (cit. on p. 15).
- Coates, Mark (2018). „RINA consulting: Subsea cable failure modes“. In: *Proceedings for subsea cable conference, London 2018*. Ed. by A. Panda (cit. on p. 20).
- DNV-GL (2014). *Guideline for installation of rigid and flexible pipelines, umbilicals and subsea power cables - Analysis*. 2014-0183, Rev. 0. DNV-GL (cit. on pp. 5, 13).
- (2016). *Guidelines for installation of rigid and flexible pipelines, umbilicals and subsea power cables - Limiting weather criteria during installation*. 2015-0964, Rev. 1. DNV-GL (cit. on pp. 3, 5).
- Eng, Y.H., W.S. Lau, G.G.L. Seet, and E. Low (2008). „Identification of the Hydrodynamics Coefficients of an Underwater Vehicle using Free Decay Pendulum Motion“. In: *Proceedings of the International MultiConference of Engineers and Computer Scientists 2008 Vol II* (cit. on p. 5).
- Guttner, W.C., C.C.P. Santos, and C.P. Pesce (2017). „A finite element method assessment of a Steel Tube Umbilical (STU) cable subjected to crushing load: Comparison between two and three-dimensional approaches“. In: *Marine Structures* 53 (cit. on p. 23).
- Hannan, M.A. and W. Bai (2015). „Nonlinear hydrodynamic responses of submerged moving payload in vicinity of a crane barge in waves“. In: *Marine Structures* 41 (cit. on p. 16).
- (2016). „Analysis of nonlinear dynamics of fully submerged payload hanging from offshore crane vessel“. In: *Ocean Engineering* 128 (cit. on p. 5).
- Holthuijsen, L.H. (2007). *Waves in oceanic and coastal water*. Cambridge University Press (cit. on pp. 13, 14).
- Journée, J.M.J., W.W. Massie, and R.H.M. Huijsmans (2015). *Offshore Hydromechanics*. Third Edition (cit. on p. 12).

- Komusanac, Ivan, Daniel Fraile, and Guy Brindley (2019). *Wind energy in Europe in 2018*. Tech. rep. WindEurope (cit. on p. 1).
- Loos, Bart (2017). „Operability limits based on vessel motions for submarine power cable installation“. MA thesis. Delft University of Technology (cit. on pp. 4, 5, 7, 36, 45).
- Maioli, P. (2016). *Measurement of flexural rigidity of submarine cables*. First South East European Regional CIGRE Conference (cit. on p. 5).
- Nakajima, Toshio, Seizo Matora, and Masataka Fujino (1982). „On the dynamic analysis of multi-component mooring lines.“ In: *Proceedings of the 14th annual Offshore Technology Conference in Houston, Texas*. (Cit. on p. 19).
- Orcaflex user manual*. Version 10.0a. Orcina (cit. on p. 27).
- Reda, A.M., G.L. Forbes, F. Al-Mahmoud, K.K. Mckee, and I.A. Sultan (2016). „Compression limit state of HVAC submarine cables“. In: *Applied Ocean Research* 56 (cit. on pp. 5, 38).
- Sarkar, Arunjyoti and O.T. Gudmestad (2010). „Splash zone lifting analysis of subsea structures“. In: *Proceedings of OMAE 2010 29th International Conference on Ocean, Offshore and Arctic Engineering* (cit. on pp. 5, 17, 18).
- Tan, Zhimin, Peter Quiggin, and Terry Sheldrake (2009). „Time Domain Simulation of the 3D Bending Hysteresis Behavior of an Unbonded Flexible Riser“. In: *Journal of offshore mechanics and Arctic engineering* 131 (cit. on p. 5).
- Technology, California Institute for. *An internet book on fluid dynamics*. Consulted at 4 december 2019. URL: <http://brennen.caltech.edu/fluidbook/externalflows/drag/dragonasphere.pdf> (cit. on p. 71).
- The Minitab blog*. Consulted at 30 march 2020. URL: <https://blog.minitab.com/blog/adventures-in-statistics-2/why-you-need-to-check-your-residual-plots-for-regression-analysis> (cit. on p. 74).
- Van den Boom, H.J.J (1985). „Dynamic behaviour of mooring lines“. In: *Beaviour of offshore structures* (cit. on p. 19).
- Walton, Thomas S. and Harry Polachek (1960). „Calculation of transient motion of submerged cables“. In: *Mathematics of computation* 14 (cit. on p. 19).
- Worzyk, Thomas (2009). *Submarine power cables*. Springer (cit. on pp. 9, 20, 22).
- Yabuta, Tetsuro (1984). „Submarine cable kink analysis“. In: *Bulletin of Japan Society of mechanical Engineers* 27 (cit. on pp. 21, 22).

# Appendices



# Vessel motion analysis Stemat Spirit

The vessel under consideration is the Stemat Spirit shown in Figure A.1, operated by Boskalis Subsea Cables. This CLV features a cable storage turntable of 4400 mT, a cable chute located off center and a crane to lift the quadrant, also located off center. The location of the suspension point for the quadrant is known and depicted in Figure A.2.



**Figure A.1.:** The Stemat Spirit CLV.

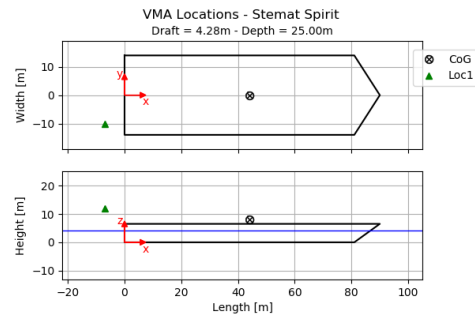


**Figure A.2.:** The location of the suspension point for the quadrant

A detailed panel model of the vessel is available within Boskalis Subsea cables. A diffraction program can therefore be used to obtain the RAOs of the vessel for a certain draught, from which the vessel response to wave excitation can quickly be calculated. This vessel motion analysis (VMA) is used to determine a set of motion parameter combinations that the vessel may reasonably be expected to encounter during operations, while still being in the vicinity of the failure criteria for the cable. Two motion criteria are used as hard safety limits for personnel activities: a maximum roll angle of  $\zeta_{4,crit} = 8 [deg]$  and a maximum heave acceleration of  $\ddot{\zeta}_{3,crit} = 3 [m/s^2]$ . Additionally, at a significant wave height of  $H_s = 3.5 [m]$  or higher the vessel discontinues operations and returns to port.

From the VMA a set of most probable maximum (MPM) displacement, velocity and acceleration values can be obtained for a range of discrete  $T_p$  values. Dividing the criteria values by the MPM values the maximum allowable  $H_s$  for that criterion is determined, see equations A.1-A.3.

$$H_s^{allowed,1} = \frac{\zeta_{4,crit}}{\zeta_{4,mpm}} \quad (A.1)$$

$$H_s^{allowed,2} = \frac{\ddot{\zeta}_{3,crit}}{\ddot{\zeta}_{3,mpm}} \quad (A.2)$$

As the first criterion to be exceeded terminates the operation the lowest  $H_s$  of the three criteria is used as the allowed  $H_s$  per case of direction and  $T_p$ , see Figure A.3.

$$H_s^{max,total} = MIN(H_s^{allowed,1}; H_s^{allowed,2}; 3.5) \quad (A.3)$$

Now that the max  $H_s$  per load case is known as well as the RAOs, the maximum occurring motion amplitude of the crane tip in the motion directions of interest (heave and sway) can be determined, see Figure A.4. Taking the maximum over the range of directions for each  $T_p$  generates a set of 14 load cases (Figure A.5) that consist of a vessel motion direction (heave and sway) and vessel motion amplitude  $\zeta$ ,  $H_s$ ,  $T_p$  and wave direction values.

Allowable $H_s$ [m]		Directions [deg]									
		-180	-135	-90	-45	0	45	90	135	180	
Tp [s]	5	3.500	3.500	3.500	3.500	3.500	3.500	3.500	3.500	3.500	3.500
	7.5	3.500	3.023	1.355	2.798	3.408	2.398	1.355	3.023	3.500	3.500
	10	3.500	3.500	2.079	3.500	3.500	3.463	2.079	3.500	3.500	3.500
	12.5	3.500	3.500	2.712	3.500	3.500	3.500	2.712	3.500	3.500	3.500
	15	3.500	3.500	3.425	3.500	3.500	3.500	3.425	3.500	3.500	3.500
	17.5	3.500	3.500	3.500	3.500	3.500	3.500	3.500	3.500	3.500	3.500
	20	3.500	3.500	3.500	3.500	3.500	3.500	3.500	3.500	3.500	3.500

Figure A.3.: Maximum  $H_s$  at which operations may continue, combining criteria for roll displacement, heave acceleration and significant wave height. Note that some directions have been omitted from this table to fit it on the page, the actual directional spacing is 15 °.

Allowable $\zeta$ [m] heave		Directions [deg]									
		-180	-135	-90	-45	0	45	90	135	180	
Tp [s]	5	0.664	1.205	1.553	1.810	1.828	2.286	2.386	1.370	0.658	0.658
	7.5	2.906	3.632	1.547	2.907	3.898	3.789	2.257	3.502	2.970	2.970
	10	4.287	4.764	2.292	3.828	4.659	5.160	2.715	4.041	4.258	4.258
	12.5	4.545	4.664	2.866	3.800	4.641	4.875	3.177	3.966	4.491	4.491
	15	4.480	4.447	3.485	3.719	4.486	4.562	3.722	3.838	4.422	4.422
	17.5	4.303	4.206	3.435	3.606	4.278	4.277	3.593	3.692	4.248	4.248
	20	4.118	3.995	3.332	3.499	4.083	4.043	3.442	3.563	4.067	4.067

Figure A.4.: Heave amplitude of the crane tip for the maximum allowable  $H_s$  per load case.

Tp [s]	Heave				Sway			
	case	$\zeta$ [m]	dir [°]	$H_s$ [m]	case	$\zeta$ [m]	dir [°]	$H_s$ [m]
5	1	2.40	75	3.35	8	1.80	105	3.50
7.5	2	3.91	-15	3.49	9	2.36	-135	3.02
10	3	5.16	45	3.46	10	3.66	-135	3.50
12.5	4	4.88	30	3.50	11	4.28	-60	3.50
15	5	4.63	30	3.50	12	4.79	60	3.50
17.5	6	4.37	30	3.50	13	5.25	60	3.50
20	7	4.15	15	3.50	14	5.72	75	3.50

Figure A.5.: Load cases derived from the VMA.

The model used in this thesis is based on the assumption that the influence of the response of the cable and quadrant on the vessel is of such minor magnitude that it can be neglected. This way the vessel motion can be simulated separately, after which the suspension point motion can be imposed on the cable-quadrant system. To determine if this is the case the moment of inertia of the vessel in pitch

( $I_{v,pitch} = 3.47 * 10^9 [kg/m^2]$ ) and roll ( $I_{v,roll} = 5.45 * 10^8 [kg/m^2]$ ) is compared to the maximum moment of inertia that the quadrant-cable system can apply to the vessel. Given a maximum quadrant load of 9 ton including self-weight and considering the location of the suspension point this yields a maximum applied moment that is approximately 19 times smaller than the moment of inertia of the vessel in the most unfavorable case. It is therefore concluded that the assumption of decoupled motions is reasonable to apply, see equations A.4-A.7.

$$I_{q,pitch} = w * g * l^2 = 9000 * 9.81 * 43.9^2 = 1.8 * 10^8 [kg/m^2] \quad (A.4)$$

$$Unity\ check\ pitch = \frac{I_{v,pitch}}{I_{q,pitch}} = \frac{3.47 * 10^9}{1.8 * 10^8} = 19.27 \quad (A.5)$$

$$I_{q,roll} = w * g * l^2 = 9000 * 9.81 * 7.82^2 = 5.4 * 10^6 [kg/m^2] \quad (A.6)$$

$$Unity\ check\ roll = \frac{I_{v,roll}}{I_{q,roll}} = \frac{5.45 * 10^8}{5.4 * 10^6} = 101 \quad (A.7)$$



## Hydrodynamic interaction

The hydrodynamic reaction to cable motion is critical in the analysis of the dynamic response of the cable-quadrant system to the excitation by the vessel motion. It consists of drag and inertia effects in both normal and axial directions of the cable. The magnitude of these coefficients depends on the flow characteristics that the cable experiences, expressed by the dimensionless Reynolds ( $Re$ ) and Keulegan-Carpenter ( $KC$ ) numbers, which are in turn derived from cable shape and environmental parameters.

$$Re = \frac{u_r D}{\nu} \quad (\text{B.1})$$

$$KC = \frac{UT}{D} \quad (\text{B.2})$$

$Re$  = Reynolds number [-]

$u_r$  = Relative velocity [ $m/s$ ]

$D$  = Diameter [ $m$ ]

$\nu$  = Kinematic viscosity [ $m^2/s$ ]

$KC$  = Keulegan Carpenter number [-]

$U$  = Velocity amplitude [ $m/s$ ]

$T$  = Period of oscillation [ $s$ ]

A typical pull-in operation might be performed in the North Sea. Given an average temperature of 10 °C at that location the kinematic viscosity of the seawater  $\nu = 1.06 \times 10^{-6} [m^2/s]$  and the diameter of the cable  $D = 0.124 [m]$ . From the VMA a set of maximum occurring motion amplitudes at given periods is acquired (appendix A). From these limits a range of maximum velocities is derived, which can be used to determine the Reynolds numbers and KC numbers.

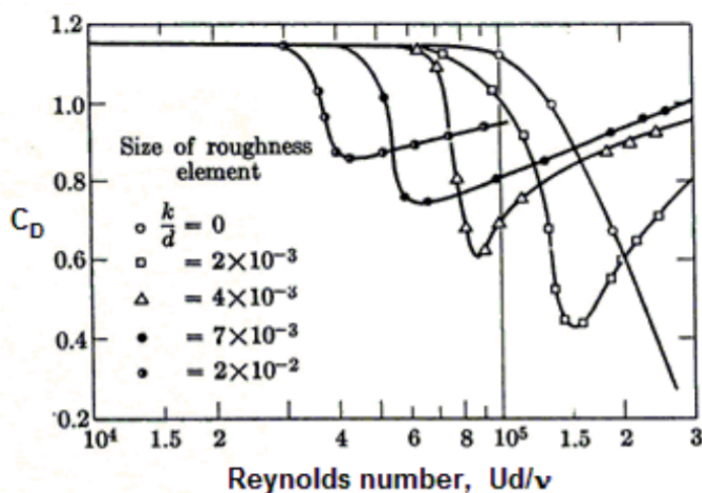


**Figure B.1.:** Normal drag coefficient for cylinders of various surface roughness values, taken from: [An internet book on fluid dynamics](#).

The outer roving of the cable is made of fine strands of polyethylene fibers, resulting in a surface roughness of  $k = 0.5$  [mm] and  $\frac{k}{d} = \frac{5 \cdot 10^{-4}}{0.124} = 4 \cdot 10^{-3}$ . For cables with a length much larger than the diameter, the friction coefficient in normal direction is equal to  $C_{d,n} = 1.2$  up to  $Re = 6 \cdot 10^4$  regardless of surface roughness because of the laminar flow pattern. At  $Re = 6 \cdot 10^4$  the drag starts to drop sharply to  $C_{d,n} = 0.6$  at  $Re = 8 \cdot 10^4$  as the flow becomes (super)critical and transitions to turbulent flow. In axial cable direction there is no frontal area as the cable is prismatic over the length. This means that the only friction present is skin friction. The axial drag coefficient is therefore much lower:  $C_{d,a} = 0.01$ .

In addition to the Reynolds number, the  $KC$  number can also be extracted from the VMA. The  $KC$  number varies in the range 90-326 in 25 m water depth for the maximum motion amplitudes making it highly drag dominated. For lower motion amplitudes the  $KC$  number may be lower, meaning neither drag nor inertia dominates and the full Morison equation is required, along with accurate inertia coefficients. The inertia coefficient is separated into two parts:  $C_I = C_f + C_a$ . The first term represents the Froude-Krylov contribution and is commonly accepted to be  $C_f = 1$ . The second term is the added mass contribution. This coefficient asymptotically approaches  $C_a = 0.9$  for a cylinder in cases in which the free surface is relatively far away (Betts Berklite, 1972). In axial direction the added inertia coefficient is assumed to be zero.

**Table B.1.:** Overview of hydrodynamic interaction coefficients. \*See Figure B.1 for full definition of the normal drag coefficient.

Property	Symbol	Value/Range	Unit
Kinematic viscosity seawater	$\nu$	$1.06 \cdot 10^{-6}$	$[m^2/s]$
Surface roughness	$k/D$	$4 \cdot 10^{-3}$	$[-]$
Reynolds number	$Re$	$2.1 - 4.5 \cdot 10^5$	$[-]$
Keulegan Carpenter number	$KC$	$90 - 326$	$[-]$
Axial drag coefficient	$C_{d,a}$	0.01	$[-]$
Normal drag coefficient	$C_{d,n}$	1.2*	$[-]$
Froude-Krylov coefficient	$C_f$	1	$[-]$
Added mass coefficient	$C_a$	0.9	$[-]$

## Statistic analysis

The performed simulations of the cable-quadrant system generate a lot of data. From each simulation a set of independent parameters and a set of dependent parameters are recorded. The independent (or input) parameters consist of the suspension point motions (displacement, velocity and acceleration) in 6 directions (heave, sway and cable axial in both positive and negative directions). The dependent parameters consist of the response of the cable-quadrant system: tension, compression and curvature. The results of the simulations are visualized in scatterplots that relate a single dependent parameter to a single independent parameter. Each data point represents the result of one simulation. Collecting the results of all the simulations with the same configurations and boundary conditions into the same figure generates a scatter of data points from which relations may be derived. The data points in the scatter plot may indicate a relation between the independent and dependent variable. This relation can be determined by applying ordinary least squares regression to the data points. This linear regression aims to generate a best fit line through the obtained data points in order to make predictions about new realizations of the model. The linear equation resulting from the regression is:

$$Y = \beta_0 + \beta_1 * X + \epsilon \quad (\text{C.1})$$

This equation relates the dependent parameter  $Y$  (output) to the independent parameter  $X$  (input) through the slope of the line  $\beta_1$ , a starting value at  $X = 0$  denoted as  $\beta_0$  and a fit error component  $\epsilon$ . Curvilinear relations will not be approximated accurately by simple linear regression. This can be solved by using polynomial (or multiple linear) regression. The result of the polynomial regression is:

$$Y = \beta_0 + \beta_1 * X + \beta_2 * X^2 + \dots + \beta_n * X^n + \epsilon \quad (\text{C.2})$$

This equation relates the output to a single input variable up to a specified order  $n$ . The higher the order the better the line fits the data. However, increasing the order too much will decrease the predictive value of the fitted curve. For the purposes of this thesis, a second order polynomial fit is applied. The polynomial is linear in the coefficients and therefore represents a linearization of the problem. The main drawback of the polynomial regression is that it is sensitive to outliers. Outliers should therefore be explained through physical processes and removed from the

data set where possible. The applicability of the fitted curved can be measured and validated using several tests. The  $R^2$  score is a measure of the closeness of the fit to the data points. It expresses to what degree the fitted model explains the position of the data points by means of a number between 0 and 1, where 1 is a perfect fit. In practice, a perfect fit never occurs, there will be residual errors on most data points with respect to the fit. While a closely fitted curve is precise, it may not be accurate. If the fitted curve has the tendency to overestimate or underestimate the data points the equation is biased. This bias decreases the predictive capacity of the model. The model may also fan out: increasing the error with the input increasing in value. This so called heteroscedasticity is a problem to the predictive value of the model near the higher input regions. In this thesis these are the areas of interest. The models should therefore be carefully checked to see this effect does not pollute the results. This can be achieved by visual inspection of the residual errors of the results. The plotted values of these residual errors should produce a random scatter of data points equally distributed around a mean of 0. If there is an observable trend in the residuals data, the model is biased as can be observed in the left plot in Figure C.1. In addition, the error should remain evenly distributed for the whole range of values of the independent variable. If the errors increase with the input, the model is heteroscedastic. This is displayed in the right plot in Figure C.1. This would potentially make the model unusable near the failure envelope.

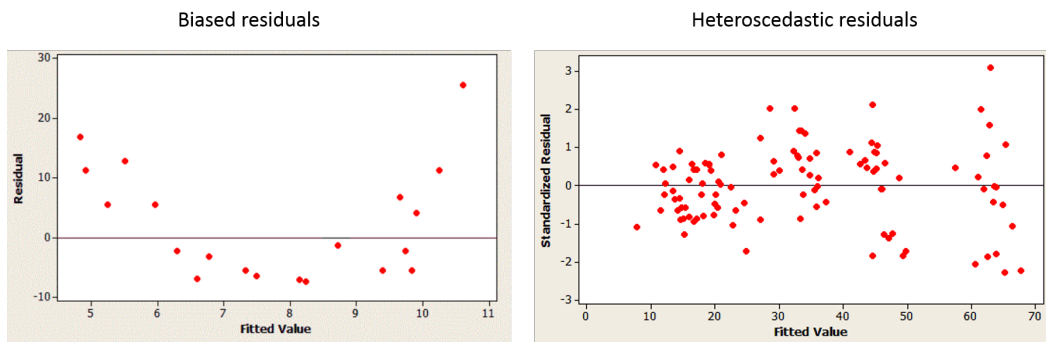


**Figure C.1.:** Examples of biased and heteroscedastic residuals plots (taken from *The Minitab blog*).

A final check is the F-test of overall significance (named after statistician Robert Fisher). This statistical test determines how significant the regression model is. Without a successful F-test, the  $R^2$  score carries little significance and the model has little predictive value. The F-test tests the chance of obtaining the results as they are, under the assumption that no relation exists. This chance is expressed as the p-value: a number between 0 and 1. A high p-value indicates that no actual relation is present in the test sample. A low p-value indicates that the obtained realizations in the test sample are the result of a physically present relation. Generally, a p-value lower than 0.05 is required to be able to report any significant relation, but a  $p < 0.01$  is desirable. Finally, for each fitted model a 95% prediction interval is plotted to indicate the uncertainty in new predictions within the input range assessed.

## Statistic significance of results

The validation steps described above are performed for the most correlated cases from Section 8.3. After fitting the curve, the residual errors are plotted to check for bias and heteroscedasticity. The p-value of the F-test has been plotted above each residual error plot. This is displayed in Figure C.2. For all cases, the p-value is extremely low. This means that the  $R^2$  values given in Chapter 8 are statistically significant. The residuals for snapshot 1 and 2 are unbiased. There is some spreading of the errors. However, the spread decreases towards the extreme input values, so there is no heteroscedasticity present. The residuals for snapshot 3 are both unbiased and homoscedastic.

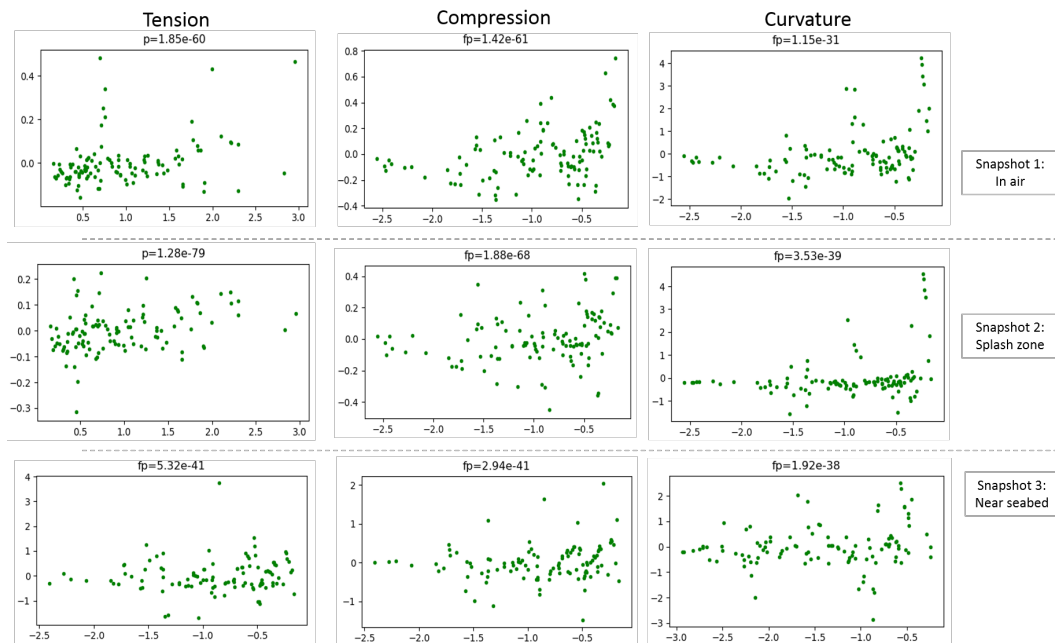


Figure C.2.: Residual error plots from the polynomial fits for the best correlated cases.



## Sensitivity study

As convenient and extensive as Orcaflex is to analyze a wide range of situations, if the input is erroneous the output will be too. To verify that the models that are applied are correct and suitable to analyze the situations of interest, a sensitivity analysis is performed. The following physical and model properties are tested to see in what way they influence the analysis and to detect what errors they could be introducing to the model:

- Pendulum length** The length of the lift wire by which the quadrant is suspended. For a normal pendulum this influences the motion response, but the influence on the system compared to that of the cable needs to be determined.
- Quadrant flooding** Whether or not the quadrant is submerged or not. A submerged quadrant is expected to decrease motion amplitudes.
- Hydrodynamic cable coefficients** For all the cases the cable is (almost) fully submerged. The hydrodynamic interaction is modeled through drag and inertia coefficients. The influence of these coefficients is investigated.
- Hydrodynamic quadrant coefficients** Like the cable, the structural elements of the quadrant are characterized by hydrodynamic coefficients. The effect of variations of these are investigated.
- Solving method** Orcaflex incorporates three possible solving methods: explicit, implicit with constant time step and implicit with variable time step. The explicit method is said to be the most stable and accurate, but the implicit methods are significantly faster. It is investigated if the implicit methods are applicable for the analyses required in this thesis.
- Segment length** The cable is discretized into segments of finite length. Increasing the amount of segments increases accuracy but increases computation times as well. The segment length is varied to find the optimal length.
- Time step size** Increasing the time step size has similar effects as increasing the segment length. A similar analysis is therefore performed on it.

## Sensitivity models

The sensitivities described above are investigated using two models. Base model 1 consists of a quadrant suspended by a lift wire of stiffness  $100 * 10^3$  [kN/m] and length of 10 [m]. The suspension point to which the lift wire is attached is subject to an imposed motion. The quadrant freely supports the cable that hangs off to both sides, touching down and stretching a length on the seabed, where the cable end is fixed after a tension of 2.5 [kN] is applied. A single side of the cable is 122 [m] long and divided into 200 sections. The calculation includes torsion stiffness, nonlinear bend stiffness and bending hysteresis. The calculation method is an implicit method with fixed time step of size 0.01 [s]. This model is used to verify the effect of pendulum length, an immersed or emerged quadrant and the effect of the hydrodynamic coefficients of the quadrant and the cable.

Base model 2 is used to assess the system sensitivity to the solving method, segmentation length and time step size. The model features the same imposed motion as base model 1, except it is directly imposed on the quadrant. Only one side of the cable hanging off the quadrant is modeled. The top end of the cable is pinned to the top of the quadrant. The boundary condition of the other end is the same as in base model 1.

## Results base model 1

From Figure D.1 and Figure D.2 it follows that a configuration in which the quadrant is submerged influences the maximum tension significantly. Note that this comparison is achieved by raising the water level to submerge the quadrant. The geometric configuration of the quadrant and cable does not change with respect to the seabed. Furthermore, Figure D.1 shows clearly that both higher  $C_D$  and  $C_I$  of the cable cause higher extreme tension values, located near and on the quadrant. The effect of changing the hydrodynamic coefficients of the structural elements of the quadrant is very small as visualized in Figure D.2.

The length of the lift wire has a profound effect on both compression and tension. A longer pendulum length increases maximum tensions as is apparent from Figure D.3. For the quadrant near the seabed this behavior changes. The pendulum length still influences the response, however the relation is less straightforward as the longest pendulum length in Figure D.4 decreases both tension and compression.

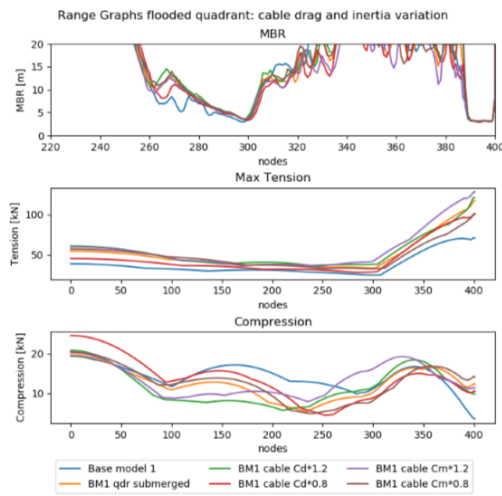


**Figure D.1.:** Range graphs for base model 1 in air subject to variations in hydrodynamic coefficients of the cable.

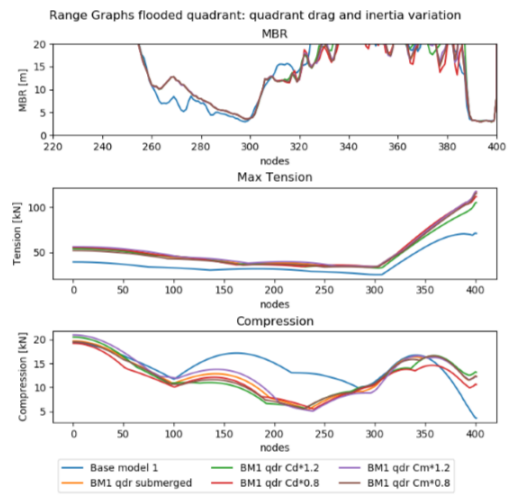


**Figure D.2.:** Range graphs for base model 1 in air subject to variations in hydrodynamic coefficients of the quadrant.

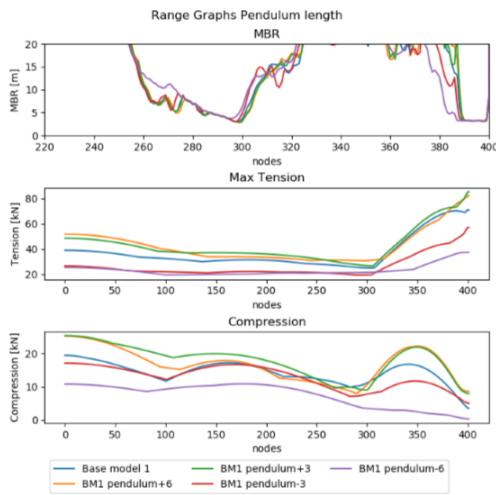


**Figure D.3.:** Range graphs for base model 1 in air subject to variations in pendulum length.

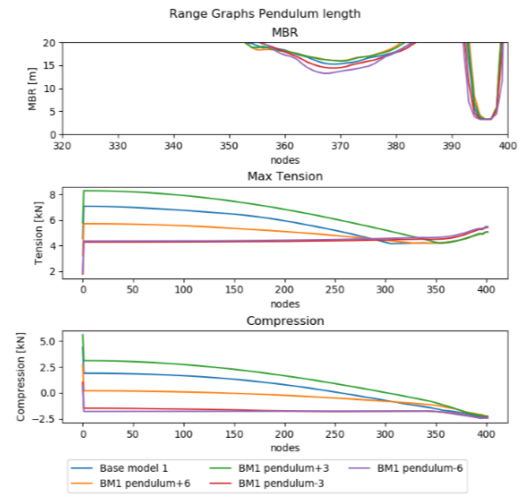


**Figure D.4.:** Range graphs for base model 1 near the seabed subject to variations in pendulum length.

## Results base model 2

Looking at Figure D.5 it can be observed that the explicit time solving method generates high compression loads compared to the other methods. This is due to high frequency oscillations that are difficult to filter out. From Figure D.6 it follows that the implicit solver achieves convergence in bending radius with time step sizes of 0.01 [s] or smaller. The variable time step solver deviates from this and is therefore discarded. The differences in compression and tension for all step sizes are predominantly due to high frequency oscillations as well. Contrary to the explicit solver, these are filtered easily by introducing seabed friction or Rayleigh damping. Varying the segment length provides a clear picture (Figure D.7): the smallest segment lengths of 0.3 and 0.15 [m] achieve the same results for bending, compression and tension. The base case deviates in bending and the larger segment sizes deviate across the board or even cause instability of the simulation.

Introducing seabed friction or Rayleigh damping generates the same results (Figure D.8), with the exception of two peaks near the quadrant. These peaks introduced by the Rayleigh damping defeat its purpose of smoothing the output and therefore only seabed friction will be used in the model, as this smooths the high frequency peaks sufficiently. The explicit method still exhibits the large spikes in compression from the high frequency noise even though seabed friction is incorporated.

Finally, in Figure D.9 the effect of the friction coefficient is depicted. The effect on bending behavior is negligible and tension is not influenced near the limits. Maximum compression is highly dependent on the magnitude of the friction coefficient.

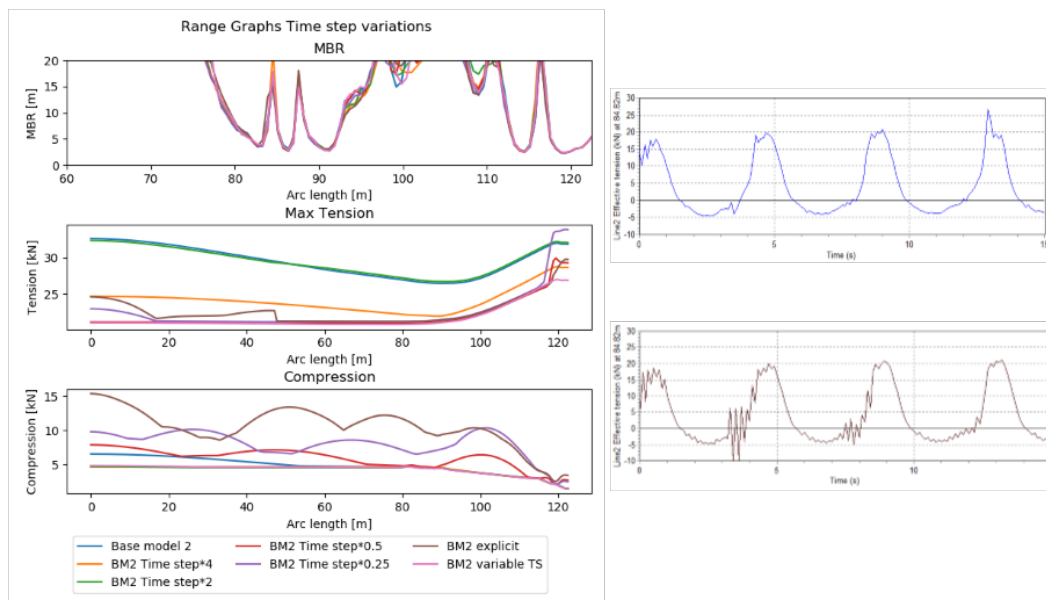


**Figure D.5.:** Range graphs (left) and time traces of the node at 85 [m] for the base case in air (top right) and the explicit solving method (bottom right).

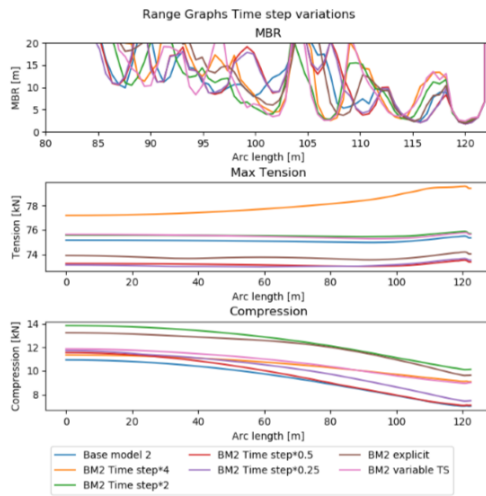


Figure D.6.: Range graphs of the model near the seabed.

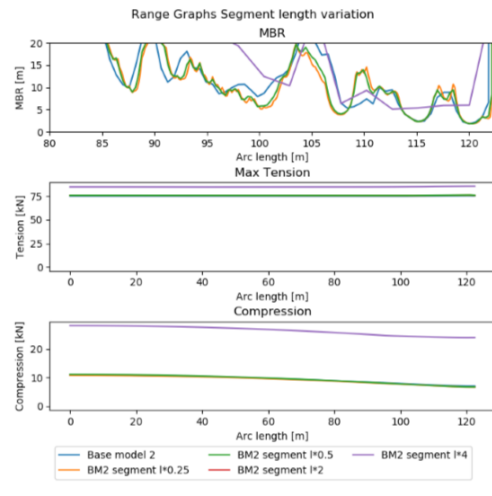


Figure D.7.: Range graphs of the model near the seabed.

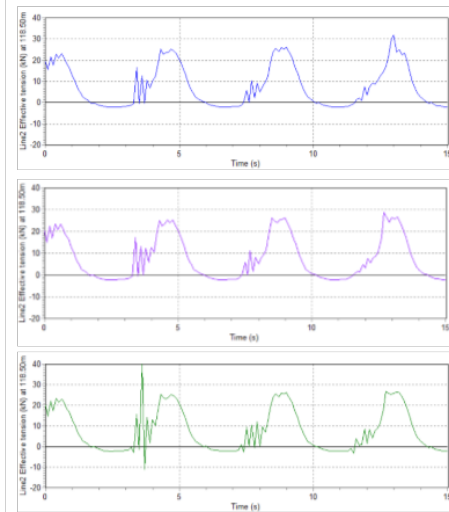
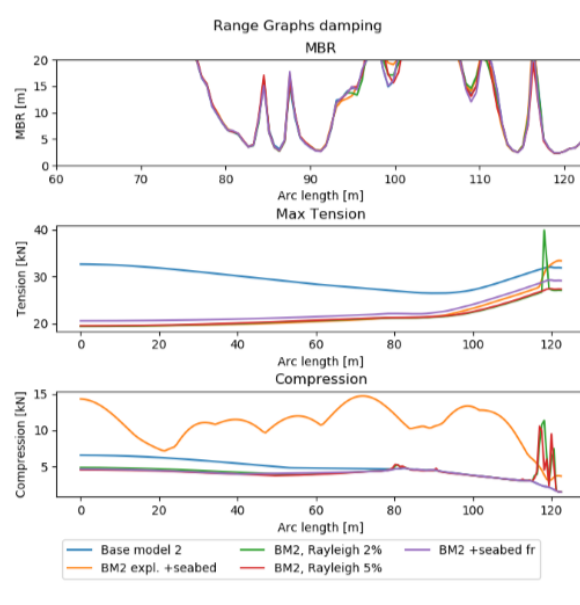


Figure D.8.: Range graphs for various damping implementations (left) and time traces for the base case (top right), the base case including seabed friction (mid right) and for Rayleigh damping at 2% (bottom right).

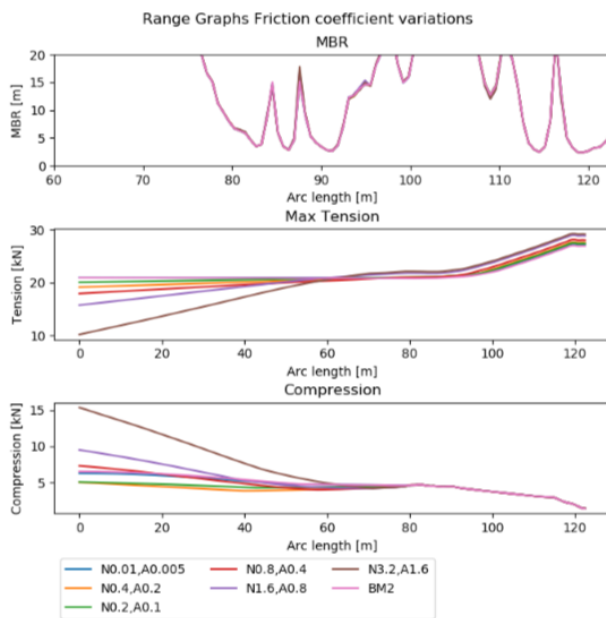


Figure D.9.: Range graphs for various friction coefficients in normal (N) and axial (A) direction.

# Glossary of terms

## List of symbols

$A$	Area perpendicular to flow [ $m^2$ ]
$C_D$	Drag coefficient [-]
$C_I$	Inertia coefficient [-]
$C_a$	Added mass coefficient [-]
$C_f$	Froude-Krylov coefficient [-]
$D$	Diameter [ $m$ ]
$F_D$	Drag force [ $N$ ]
$F_I$	Inertia force [ $N$ ]
$F_t$	Axial cable tension
$H_s$	Significant wave height [ $m$ ]
$KC$	Keulegan Carpenter number [-]
$L$	Pendulum length [ $m$ ]
$R$	Radius [ $m$ ]
$Re$	Reynolds number [-]
$T$	Period of oscillation [ $s$ ]
$T_d^+$	Max. dynamic tension [ $kN$ ]
$T_s^+$	Max. static tension [ $kN$ ]
$T_d^-$	Min. dynamic tension [ $kN$ ]
$T_s^-$	Min. static tension [ $kN$ ]
$T_0$	Bottom tension force [ $N$ ]
$T_i$	Tension in segment $i$ [ $N$ ]
$T_p$	Peak period [ $s$ ]
$U$	Velocity amplitude [ $m/s$ ]
$V$	Volume [ $m^3$ ]
$X_{ct}$	X position of crane tip relative to CoG [ $m$ ]
$Z_{ct}$	Z position of crane tip relative to CoG [ $m$ ]
$\alpha$	Segment angle [deg]
$\alpha$	Phase angle [rad]
$\bar{F}_c$	Normalized compression [-]
$\bar{T}$	Normalized tension [-]
$\bar{\kappa}$	Normalized curvature [-]
$\chi$	Vessel roll [deg]
$\eta$	Surface elevation [ $m$ ]
$\kappa_d^+$	Max. dynamic curvature [ $1/m$ ]
$\kappa_s^+$	Max. static curvature [ $1/m$ ]
$\nu$	Kinematic viscosity [ $m^2/s$ ]

$\omega$	Radial frequency [ <i>rad/s</i> ]
$\omega_0$	Payload natural frequency [ <i>rad/s</i> ]
$\phi$	Vessel pitch [deg]
$\psi$	Vessel yaw [deg]
$\rho$	Density [ <i>kg/m<sup>3</sup></i> ]
$\rho_w$	Density of sea water [ <i>kg/m<sup>3</sup></i> ]
$\theta$	Average node angle [deg]
$\theta$	Wave direction angle [°]
$\xi$	Vessel surge [ <i>m</i> ]
$\zeta$	Wave amplitude [ <i>m</i> ]
$\zeta$	Vessel heave [ <i>m</i> ]
$a$	Acceleration [ <i>m/s<sup>2</sup></i> ]
$a$	Catenary parameter [ <i>m</i> ]
$a_f$	Acceleration relative to fixed reference [ <i>m/s<sup>2</sup></i> ]
$a_n$	Normal added mass [ <i>kg</i> ]
$a_t$	Tangential added mass [ <i>kg</i> ]
$b$	width between crane tip and CoG [ <i>m</i> ]
$d$	Water depth [ <i>m</i> ]
$g$	Gravitational acceleration [ <i>m/s<sup>2</sup></i> ]
$h$	height between crane tip and CoG [ <i>m</i> ]
$i$	Frequency index [-]
$i$	Node and segment index
$j$	Directional index [-]
$k$	Wave number [ <i>rad/m</i> ]
$l$	Segment length [ <i>m</i> ]
$l$	length between crane tip and CoG [ <i>m</i> ]
$m$	Mass [ <i>kg</i> ]
$m_a$	Added mass [ <i>kg</i> ]
$t$	Time [ <i>s</i> ]
$u_r$	Relative velocity [ <i>m/s</i> ]
$w$	Submerged cable weight [ <i>kg/m</i> ]
$x$	X coordinate [ <i>m</i> ]
$y$	Y coordinate [ <i>m</i> ]
$z$	Z coordinate [ <i>m</i> ]
°C	Degrees Celsius

## Acronyms

<b>AC</b>	alternating current
<b>CLV</b>	cable lay vessel
<b>CPS</b>	cable protection system
<b>DC</b>	direct current
<b>DOF</b>	degree of freedom
<b>HVAC</b>	high voltage alternating current
<b>JIP</b>	joint industry project

<b>LMM</b>	lumped mass method
<b>MBR</b>	minimum bending radius
<b>MPM</b>	most probable maximum
<b>PE</b>	polyethylene
<b>RAO</b>	response amplitude operator
<b>SWP</b>	side-wall pressure
<b>TDP</b>	touchdown point
<b>VMA</b>	vessel motion analysis
<b>XLPE</b>	cross linked polyethylene

## Terminology

<b>catenary</b>	The curve that a wire, chain, cable or rope assumes under its own weight when it is supported at the ends.
<b>operability</b>	Limiting conditions at which a certain activity can be performed.
<b>pitch</b>	Lay angle of the helical armoring wires in the cable.
<b>quadrant</b>	Semicircular guide frame on which the excess length of cable is suspended during the 2 <sup>nd</sup> end pull-in.
<b>stick-slip</b>	Sliding behavior between two surfaces where the friction transitions from static to dynamic friction and vice versa.
<b>swell</b>	A sea state in which the waves are generated by wind far away from the assessment location. Swell is characterized by a short range of wave components resulting in a narrow spectral peak.
<b>wind-sea</b>	A sea state in which the waves are locally generated by wind. It is characterized by a large number of wave components resulting in a wide spectral peak.
<b>workability</b>	The amount of time conditions are suitable for an activity to be performed.



## List of Figures

2.1	Flowchart of the analysis process. . . . .	6
3.1	Snapshot A . . . . .	7
3.2	Snapshot B . . . . .	7
3.3	Snapshot C . . . . .	8
3.4	Snapshot D . . . . .	8
3.5	Snapshot E . . . . .	8
3.6	DC cable structure (courtesy of Nexans). . . . .	9
3.7	AC cable structure (courtesy of Nexans). . . . .	9
3.8	Nonlinear bending stiffness implemented in this thesis. . . . .	10
3.9	Quadrant . . . . .	12
3.10	Variance density spectrum of an irregular sea state incorporating a narrow swell peak and a widely spread wind-sea peak, taken from (Holthuisen, 2007, p. 48). . . . .	14
4.1	12 DOF crane-cargo system (taken from Cha et al. 2010) . . . . .	15
4.2	Drag coefficients for linear elements. . . . .	15
4.3	Horizontal motions of payload in the presence of a fixed crane vessel. The low frequency component for the case of upstream beam loading is the natural frequency contribution, the high frequency component is the wave frequency and the negative mean signifies the mean drift force as a result of the interaction between the payload and the vessel. Picture taken from Hannan and Bai 2015. . . . .	16
4.4	Added mass for a flat object near the free surface as suggested by Sarkar and Gudmestad 2010. . . . .	18
4.5	Normalized added mass of a cylinder near the free surface (solid line) and the normalized rate of change (dotted line), illustration taken from: Sarkar and Gudmestad 2010. . . . .	18
4.6	Catenary graph . . . . .	19
4.7	Discretization . . . . .	19
4.8	Birdcaging. . . . .	21
4.9	Cable kink formation process, taken from (Yabuta, 1984). . . . .	21

5.1	Reduction of the wave time trace from a long record to 150 seconds around the highest rise or fall <u>velocity</u> . This time trace is then applied to the full model including the cable and quadrant to keep computational intensity manageable. . . . .	26
5.2	LMM discretisation (taken from <i>Orcaflex user manual</i> ). . . . .	27
5.3	Full LMM method as used by Orcaflex (taken from <i>Orcaflex user manual</i> ). . . . .	27
5.4	Example operability plot for a second end pull-in operation depicting operable $H_s$ , $T_p$ and direction combinations for a given vessel and water depth $d$ . . . . .	29
6.1	Analysis process schematization: sea state determination, vessel motion analysis, suspension point motion, cable response, curve fitting and limit statements. . . . .	31
6.2	General static configuration of the cable-quadrant system suspended on the vessel crane tip. In the dynamic analysis it is subject to direct sea state loading on the quadrant and the cable, as well as to crane tip motion (as generated by the vessel motions which in turn are generated by the sea state). . . . .	32
6.3	Three snapshots that are considered in this thesis: 1. The quadrant is suspended above the water; 2. The quadrant is situated just below the surface; 3. The quadrant is near the seabed. . . . .	33
6.4	Sea state selection diagram. . . . .	34
6.5	Load cases derived from the VMA. . . . .	34
6.6	Directional convention with the static configuration of the cable on the quadrant as a reference. . . . .	36
6.7	Example of a scatter plot. It displays the normalized tension in relation to the heave velocity for snapshot 2. Plotted along with the data points are the fitted polynomial regression line labeled with a goodness of fit score, and a 95% prediction interval for new data points based on this data. The different colored data points indicate JONSWAP spectrum versus Airy wave cases. . . . .	37
7.1	The Orcaflex model for snapshot 2. . . . .	39
7.2	Location of the suspension point. . . . .	40
7.3	Geometric model of the quadrant. . . . .	40
7.4	Catenary position after Newton Raphson iteration with perturbed initial estimate based on analytic catenary. . . . .	43
7.5	Catenary tension as determined by the catenary equation, NR-iteration and orcaflex model. . . . .	43
8.1	Results from the current investigation (left) and that of previous work (right, taken from (Loos, 2017)). . . . .	45
8.2	Comparison between JONSWAP and Airy waves for a case with low correlation between input and output (left) and a case with close correlation (right). Both panels display results for snapshot 2: splash zone. . . . .	46

8.3	Comparison between curve fits for output parameter correlation to positive and negative input. . . . .	46
8.4	Tension related to different input motions for snapshot 2. The correlation with heave is the closest. . . . .	47
8.5	Mechanical cable response as a function of suspension point motion in <b>positive</b> motion direction for the most correlated cases based on the $R^2$ score. . . . .	48
8.6	Mechanical cable response as a function of suspension point motion in <b>negative</b> motion direction for the most correlated cases based on the $R^2$ score. . . . .	48
8.7	Mechanical cable response as a function of suspension point motion including the normalized limits. Only the most correlated cases are displayed. The outliers due to resonance described in Section 8.3 as well as the low frequency outliers have been removed. . . . .	49
8.8	Mechanical cable response as a function of suspension point motion including the normalized limits. Only the most correlated cases are displayed. The outliers due to resonance described in Section 8.3 have been removed. . . . .	50
8.9	Direct wave loading effect for snapshot 1 on the relation between downward heave velocity and curvature. . . . .	50
8.10	Direct wave loading effect for snapshot 2 on the relation between downward heave velocity and curvature. . . . .	51
8.11	Direct wave loading effect for snapshot 3 on the relation between downward heave velocity and compression. . . . .	51
8.12	Direct wave loading effect for snapshot 2 on the relation between downward heave displacement and curvature. . . . .	51
8.13	Parameter variation effect on compression. . . . .	52
8.14	Parameter variation effect on curvature. Only the most correlated relations are shown. . . . .	53
A.1	The Stemat Spirit CLV. . . . .	67
A.2	The location of the suspension point for the quadrant . . . . .	67
A.3	Maximum $H_s$ at which operations may continue, combining criteria for roll displacement, heave acceleration and significant wave height. Note that some directions have been omitted from this table to fit it on the page, the actual directional spacing is $15^\circ$ . . . . .	68
A.4	Heave amplitude of the crane tip for the maximum allowable $H_s$ per load case. . . . .	68
A.5	Load cases derived from the VMA. . . . .	68
B.1	Normal drag coefficient for cylinders of various surface roughness values, taken from: <a href="#">An internet book on fluid dynamics</a> . . . . .	71
C.1	Examples of biased and heteroscedastic residuals plots (taken from <a href="#">The Minitab blog</a> ). . . . .	74
C.2	Residual error plots from the polynomial fits for the best correlated cases. . . . .	75

D.1	Range graphs for base model 1 in air subject to variations in hydrodynamic coefficients of the cable. . . . .	79
D.2	Range graphs for base model 1 in air subject to variations in hydrodynamic coefficients of the quadrant. . . . .	79
D.3	Range graphs for base model 1 in air subject to variations in pendulum length. . . . .	79
D.4	Range graphs for base model 1 near the seabed subject to variations in pendulum length. . . . .	79
D.5	Range graphs (left) and time traces of the node at 85 [m] for the base case in air (top right) and the explicit solving method (bottom right). . .	80
D.6	Range graphs of the model near the seabed. . . . .	81
D.7	Range graphs of the model near the seabed. . . . .	81
D.8	Range graphs for various damping implementations (left) and time traces for the base case (top right), the base case including seabed friction (mid right) and for Rayleigh damping at 2% (bottom right). . .	81
D.9	Range graphs for various friction coefficients in normal (N) and axial (A) direction. . . . .	82

## List of Tables

3.1	Representative properties of inter-array cables. The values presented here will be used throughout this thesis. . . . .	11
3.2	Properties of 3.2 m MBR quadrant (BSCF, 2018) . . . . .	12
6.1	High, middle and low limits for the mechanical cable failure parameters.	38
6.2	Parameter variations. . . . .	38
7.1	Vessel model properties. . . . .	40
7.2	Quadrant properties. . . . .	40
7.3	System parameters obtained from convergence study. . . . .	44
7.4	Implemented drag, inertia and seabed friction coefficients. *Value depends on $Re$ (see Figure B.1). . . . .	44
B.1	Overview of hydrodynamic interaction coefficients. *See Figure B.1 for full definition of the normal drag coefficient. . . . .	72



## Colophon

This thesis was typeset with  $\text{\LaTeX}2_{\epsilon}$ . It uses the *Clean Thesis* style developed by Ricardo Langner. The design of the *Clean Thesis* style is inspired by user guide documents from Apple Inc.

Download the *Clean Thesis* style at <http://cleanthesis.der-ric.de/>.

